In-depth profiling of calcite precipitation by environmental bacteria reveals fundamental mechanistic differences with relevance to application

Bianca J. Reeksting[1], Timothy D. Hoffmann[1], Linzhen Tan[2], Kevin Paine[2] and Susanne Gebhard[1]*

[1]Department of Biology and Biochemistry, Milner Centre for Evolution, and [2] BRE Centre for Innovative Construction Materials, University of Bath, Claverton Down, Bath, BA2 7AY, United Kingdom

Running title: Calcite precipitation by environmental bacteria

Key words: ureolysis, self-healing concrete, microbial-induced calcite precipitation, *Bacillus*

*Author for correspondence. Tel: +44 (0) 1225-386421 Email: s.gebhard@bath.ac.uk

ORIGINALITY-SIGNIFICANCE STATEMENT

Biomineralisation triggered by bacteria is important in the natural environment but also has many applications in industry, civil and geotechnical engineering. The diversity of biomineralization capability of environmental bacteria is, however, not well understood and the full potential for exploitation might therefore remain underestimated. This study surveyed environmental bacteria for their ability to precipitate calcium carbonate minerals and investigated both the mechanism and the resulting crystals. We show that while urease activity leads to the fastest precipitation, it is by no means essential. Importantly, the same quantities of calcium carbonate are produced by non-ureolytic bacteria, and the resulting crystals appear to have larger volumes and more organic components, which is likely beneficial in specific applications. This study also compares the performance of both precipitation mechanisms in a self-healing concrete application, with non-ureolytic bacteria delivering the more robust results. To our knowledge, this is the first systematic study into the fundamental differences in biomineralization between environmental bacteria and provides important information for the design of bacteria-based engineering solutions.

SUMMARY

Microbial-induced calcite precipitation (MICP) has not only helped to shape our planet's geological features, but is also a promising technology to address environmental concerns in civil engineering applications. However, limited understanding of the biomineralization capacity of environmental bacteria impedes application. We therefore surveyed the environment for different mechanisms of precipitation across bacteria. The most fundamental difference was ureolytic ability, where urease-positive bacteria caused rapid, widespread increases in pH, while non-ureolytic strains produced such changes slowly and locally. These pH shifts correlated well with patterns of precipitation on solid media. Strikingly, while both mechanisms led to high levels of precipitation, we observed clear differences in the precipitate. Ureolytic bacteria produced homogenous, inorganic fine

crystals, whereas the crystals of non-ureolytic strains were larger with a mixed organic/inorganic composition. When representative strains were tested in application for crack healing in cement mortars, non-ureolytic bacteria gave robust results, while ureolytic strains showed more variation. This may be explained by our observation that urease activity varied between growth conditions, or by the different nature and therefore material performance of the precipitate. Our results shed light on the breadth of biomineralization activity among environmental bacteria, an important step towards the rational design of bacteria-based engineering solutions.

INTRODUCTION

Environmental protests worldwide have highlighted a growing demand for action on the threat of climate change. Human activity has greatly contributed to global warming, currently causing an estimated 0.2°C increase per decade due to past and ongoing emissions (Intergovernmental panel on climate change (IPCC) 2018 report). There is a clear need to reduce our carbon dioxide (CO_2) emissions as well as to find novel ways in which we can consume CO_2 as a means of decreasing overall levels. Geological sequestration of CO_2 from large point source emitters into carbonate minerals, such as dolomite and limestone, is an emerging technology that could mitigate increasing CO_2 concentrations (Mitchell *et al.*, 2010). Microorganisms can act as biomediators to enhance carbon capture (Mitchell *et al.*, 2010) by microbial induced calcite precipitation (MICP). This process leads to precipitation of CO_2 as calcium carbonate ($CaCO_3$) as a result of microbial metabolism and has been occurring on a geological scale for more than 2.5 billion years (Altermann *et al.*, 2006). The formation by microbes of mineral carbonate structures, termed microbialites, is mediated by a large diversity of microorganisms, often working together in a consortium (Wilmeth *et al.*, 2018). Indeed, cyanobacteria in association with heterotrophic bacteria are thought to be the principal contributors to the production of carbonate rocks during almost 70% of Earth's history (3.5-0.5 Ga) (Altermann *et al.*, 2006).

The success of MICP in biological engineering of the environment has led to the investigation of its potential for exploitation in other areas. These areas include bioremediation of heavy-metal contaminated soils via immobilisation of metals in precipitates (Achal *et al.*, 2011; Ceci *et al.*, 2018), or wastewater treatment using this technology to remove excess calcium. Geotechnical engineering represents another area of interest, where MICP can improve soil properties by precipitating $CaCO_3$ to bind sand particles together. Utilizing MICP in the construction industry is another rapidly emerging field. The production and maintenance of concrete bears heavy environmental and economic costs, with cement production contributing up to 5-8 % of global anthropogenic CO_2 emissions

(Huntzinger and Eatmon, 2009; Souto-Martinez *et al.*, 2018). Moreover, reinforced concrete structures face durability issues caused by cracking and subsequent ingress of water and ions, such as chlorides. This leads to corrosion of internal steel reinforcement and eventual structural failure. MICP can seal such cracks in concrete and reduce permeability to damaging substances, thereby extending the lifespan of structures and reducing the environmental burden caused by construction of replacement structures. This broad range of applications necessitates an understanding of how bacteria precipitate calcite and what the factors are that may limit their performance.

Most bacteria are capable of MICP under suitable conditions (Boquet *et al.*, 1973), with key factors such as calcium concentration, concentration of dissolved inorganic carbon (DIC), pH, and availability of crystal nucleation sites affecting precipitation (Hammes and Verstraete, 2002). Bacterial metabolism results in an increase in both pH and DIC (through aerobic or anaerobic oxidation of organic compounds), and changes in solution chemistry (Power *et al.*, 2011). This can lead to the oversaturation of Ca^{2+} and CO_3^{2-} ions to facilitate the formation of calcium carbonate precipitates (Power *et al.*, 2011). The negatively charged cell surfaces of bacteria further promote precipitation by attracting calcium ions and acting as nucleation sites for crystal formation (Zhu *et al.*, 2016).

To date, the majority of studies of MICP have focussed on ureolytic bacteria (Zhu *et al.*, 2016). These are associated with high rates of $CaCO_3$ precipitation (Mitchell *et al.*, 2010), caused by hydrolysis of urea ($CO(NH_2)_2$) to ammonia (NH_3) and carbonic acid (H_2CO_3) (Mitchell *et al.*, 2010). The reaction of ammonia with water to ammonium (NH_4^+) and hydroxide ions (OH^-) causes an upshift in pH, while carbonic acid dissociates to generate bicarbonate (HCO_3^-). In the presence of calcium, this leads to the formation of a calcium carbonate ($CaCO_3$) precipitate (Equations 1 and 2).

$$CO(NH_2)_2 + 2H_2O \rightarrow 2NH_4^+ + CO_3^{2-} \quad (1)$$

$$Ca^{2+} + CO_3^{2-} \rightarrow CaCO_3\ (s) \quad (2)$$

Ureolytic MICP has been used in a range of applications. Positive outcomes were obtained in the improvement of soil properties, however non-uniform rates of precipitation throughout the samples led to varying results (Zhao *et al.*, 2014). In addition, the requirement for injection of the healing agent into the ground created problems where the rapid precipitation initiated by urease activity caused clogging at the injection site (Cheng and Cord-Ruwisch, 2014). In other applications, such as crack sealing in cementitious materials, ureolytic MICP has been shown to promote healing (Bang *et al.*, 2010; Wang *et al.*, 2012). However, because of the dependency of the reaction on enzymatic activity, factors such as low temperature markedly decreased the efficiency of the reaction (Wang *et al.*, 2017). In addition, ureolytic MICP requires the presence of urea, which may not always be feasible to provide, and the release of ammonia could contribute to environmental nitrogen loading (Jonkers *et al.*, 2010).

To work around the challenges associated with ureolytic bacteria, the use of other metabolic pathways needs consideration. The high efficiency of ureolytic MICP has resulted in the assumption that non-ureolytic pathways cannot yield similarly high levels of precipitation and are thus an inferior strategy to achieve precipitation. This has limited our understanding of alternative pathways, and the factors affecting efficient calcite precipitation in non-ureolytic bacteria are not clear. Studies on self-healing concrete using alkaliphilic non-ureolytic bacteria, such as *Bacillus pseudofirmus* and *Bacillus cohnii*, have shown great promise and have led to similar levels of self-healing at the laboratory scale as ureolytic bacteria (Sharma *et al.*, 2017; Alazhari *et al.*, 2018). To fully assess the potential of MICP for industrial and environmental use, detailed understanding of the microorganism, mechanism of precipitation, and application is therefore important.

Most studies of MICP have focussed on a small number of species and have thus restricted our understanding of the mechanisms of precipitation across bacteria. In addition, many previous studies have been primarily application-driven and have not always explored the deeper workings of how the bacteria precipitate minerals and what influences this ability. To

131 build a strong basis on which to develop our understanding of MICP, we here took a broad
132 view and surveyed in detail the ability of environmental bacteria to precipitate calcite.
133 Focussing on bacteria that could grow in the alkaline conditions typical of high-calcium
134 environments, we assessed the prevalence of MICP capability in environmental bacteria,
135 their mechanisms of precipitation and resulting crystal morphologies as well as their
136 suitability for application in self-healing concrete. Our study provides an understanding of the
137 environmental potential for MICP, which is not only relevant to geomicrobiology but will
138 facilitate a more design-based approach to industrial application of MICP.

139

140 **RESULTS AND DISCUSSION**

141 **Calcite precipitation ability of environmental isolates**

142 To gain a broader understanding of the capability of bacteria to precipitate calcium
143 carbonate, we first performed a survey of a range of environments. In this, we focussed on
144 sites expected to be calcium-rich, such as exposed limestone, caves and soils in areas with
145 a limestone bedrock within the southwestern United Kingdom. Our isolation strategy targeted
146 spore-forming bacteria, as their stress tolerance makes them more universally useful in
147 potential applications. Moreover, as many of the high-calcium environments are in the
148 alkaline pH range, we specifically sought for isolates that tolerate such conditions.
149 Interestingly, the majority (89 %) of colonies obtained during primary isolations had visible
150 crystal formation on the surface, indicative of biomineralization. This supports previous
151 observations that this is a common trait among bacteria (Boquet *et al.*, 1973). Of 74 isolates
152 able to grow at pH 9, 31 displayed some growth at pH 10 on 0.25x B4 minimal medium and
153 were chosen for further characterisation.

154 Preliminary identification based on partial sequencing of the 16S rDNA assigned all of the
155 isolates into Bacillales (Fig. 1). The selection of spore-formers by heat-treatment can
156 account for the prevalence of Bacillales, with most isolates grouping within the *Bacillus*

genus. The predominant species represented were *Bacillus licheniformis* and *Bacillus muralis*. *Sporosarcina pasteurii* was included in the analyses as it represents the paradigm organism for industrial application of calcite precipitation. Interestingly, five of our isolates grouped within the same clade as *S. pasteurii* (Fig. 1).

Mechanistic differences in calcite precipitation between isolates

The isolation strategy, with the exception of looking for alkali-tolerant spore formers, was unbiased for particular metabolic properties of the bacteria. A key feature of many known calcite precipitators is ureolysis, which leads to a rapid pH change in the environment due to the release of ammonia and subsequent production of OH^-. We therefore tested each of our isolates for their ability to cleave urea, which is visible as a pink colour change in test broth containing urea and phenol red (Fig. 2 and Fig. S2). Five out of the 31 isolates taken forward for further characterisation were ureolytic. Two of these ureolytic isolates (CG4_2 and CG6_1) were most closely related to *B. muralis* whilst two others (CG7_2 and CG7_3) were identified as *Lysinibacillus fusiformis*. The final isolate (EM1) was identified as *Psychrobacillus psychrodurans* and was most closely related to *S. pasteurii*. With the exception of CG4_2 and CG6_1, the other ureolytic isolates formed a monophyletic clade with the strongly ureolytic *S. pasteurii* (Fig. 1).

To determine the effects of ureolysis and the associated pH change on crystal formation, we repeated the experiment on solid media. Non-ureolytic strains showed only small changes in pH, as indicated by local colour changes in the immediate vicinity of the bacterial colony, due to general metabolic activity (Fig. 2, isolate RC1_1; Fig. S2). In contrast, a rapid and wide-spread increase in pH was apparent in the model ureolytic bacterium *S. pasteurii*. Indeed, an increase in pH as indicated by a colour change from orange to pink was visible as early as 1 h after inoculation of the plate with *S. pasteurii*, and the pH of the entire plate was alkaline by 24 h (Fig. 2). Similarly, the closely related ureolytic isolate CG7_3 caused a rapid increase in

183 pH, although the rate of pH change was slightly slower than seen in *S. pasteurii* (Fig. 2). The
184 same behaviour was observed for isolate EM1 (Fig. S2).

185 We next investigated the patterns of calcium carbonate precipitation on the same agar plates
186 and found that crystal formation correlated well with pH changes within the media. In non-
187 ureolytic strains, crystals were visible only on the surface of the colony, corresponding to the
188 observed localised pH change (Fig. 3A). In contrast, with ureolytic strains crystal
189 precipitation reflected the global pH change and occurred throughout the media (Fig. 3B).
190 The precipitation of calcium carbonate crystals throughout the media was likely due to a
191 change in the saturation kinetics in the media, resulting from the rapid increase in pH caused
192 by the urease-mediated release of ammonia from urea. Indeed, when urea was omitted for
193 isolate CG7_3, only the localised pH changes associated with non-ureolytic isolates was
194 seen (Fig. S3). In addition, crystals were only visible on the surface of the colony when urea
195 was omitted (Fig. S4), indicating that there are mechanistic differences in calcite precipitation
196 under ureolytic and non-ureolytic conditions.

197 Interestingly, two isolates that had tested positive for ureolysis in the test broth, CG6_1 and
198 CG4_2, did not produce the characteristic rapid rise in pH and associated crystal
199 precipitation when grown on solid media (Fig. 2 and S2). A possible explanation for this
200 discrepancy might be that in these isolates, urease activity is inducible in response to a cue
201 that was present in test broth, but not in the solid media. The main difference between the
202 two media was the content of nitrogen, which was very low in urease test broth (0.01 % (w/v)
203 yeast extract, 2 % (w/v) urea), but high in the solid media (0.2 % (w/v) yeast extract, 0.5 %
204 (w/v) peptone, 1 % (w/v) Lab-Lemco powder, 2 % (w/v) urea). Nitrogen metabolism and
205 urease production are tightly controlled in bacteria (Mobley and Hausinger, 1989). One
206 mechanism of regulation of urease is by repression of activity in the presence of ammonia-
207 or nitrogen-rich compounds and derepression of synthesis when nitrogen levels are low
208 (Mobley and Hausinger, 1989). We therefore tested to see whether nitrogen levels in the
209 media were having an effect on urease activity in these strains. Isolate CG6_1 was grown in

210 the presence of urea in media with either low (0.02 % yeast extract, 0.0125 % peptone, 2 %
211 urea) or high (0.2 % yeast extract, 0.125 % peptone, 2 % urea) nitrogen content, and urease
212 activity was quantified (Fig. 4A). Urease activity in CG6_1 was high when grown in low
213 nitrogen conditions, whilst significantly lower levels were detected in high nitrogen
214 conditions. This suggests that urease is only active in CG6_1 when the nitrogen supply is
215 limited. This is clearly a distinct type of behaviour from that seen in CG7_3 and *S. pasteurii*,
216 which both utilise urea rapidly regardless of the nitrogen composition of the media (Fig. 2).
217 However, while the overall urease activity of CG7_3 appeared similar to that of *S. pasteurii*
218 on solid media (Fig. 2), this isolate can grow well in the absence of urea (Fig. S3 and S4),
219 while *S. pasteurii* cannot. This suggests that CG7_3 may also be able to control the
220 expression of its urease genes, with urea acting directly as an inducer of urease activity. We
221 therefore tested the activity of whole cells grown in low and high nitrogen conditions as
222 before, but also compared cells grown in the presence and absence of urea (Fig. 4B). When
223 CG7_3 was grown in the absence of urea, it displayed medium urease activity under low
224 nitrogen conditions, which was further repressed by high nitrogen conditions. However,
225 when cells were grown in the presence of urea, urease activity was high regardless of
226 nitrogen conditions. Therefore, while urease activity in CG7_3 did show a partial response to
227 nitrogen limitation, this was overcome by incubation with urea, which clearly acted as the
228 main inducer and may be the preferred nitrogen source for this bacterium under the chosen
229 growth conditions. Taken together, our results indicate that there is a continuum of ureolytic
230 activity in environmental bacteria and that this, as seen above (Fig. 2-3), will have an impact
231 on crystal formation and biomineralization by different isolates.

232

233 **Effect of ureolysis on crystal formation**

234 Having established that crystal formation on solid media is very different between ureolytic
235 and non-ureolytic strains and that there are notable variations in ureolytic activity between
236 environmental isolates, we wanted to understand how ureolysis influences crystal formation

237 in more detail. To investigate this, we studied the kinetics of precipitation in our set of
238 isolates. Growing isolates in liquid culture with calcium over several days allowed us to
239 monitor the rates and total amounts of precipitate formed and correlate this to bacterial
240 growth and global pH changes. Growth of ureolytic isolates caused rapid alkalinisation of the
241 media, reaching pH 9 within two days, the first time point assayed. This resulted in complete
242 precipitation of the available calcium in the media on the same time-scale, with no further
243 change observed in two weeks of incubation (Fig. 5A and Fig. S5, *S. pasteurii*). Growth of
244 non-ureolytic bacteria caused a more gradual increase in pH, approaching pH 9 only in the
245 second week of incubation (Fig. 5B and Fig. S5). Precipitation of calcium in the media was
246 also more gradual, although both ureolytic and non-ureolytic isolates attained the maximum
247 theoretical levels of precipitation by the end of the first week. Strikingly, we observed
248 noticeable differences in cell numbers over the experimental period. Viable cell counts
249 decreased dramatically in ureolytic isolates and were undetectable within two days (Fig. 5A),
250 likely due to high ammonia concentrations in the media of these isolates resulting from the
251 cleavage of urea. Alternatively, these cells may have been encased by calcium carbonate,
252 preventing their further growth and division. In contrast, for non-ureolytic isolates cell
253 numbers gradually increased, before declining again over prolonged incubation (Fig. 5B).
254 These differences in viability over time between ureolytic and non-ureolytic bacteria may
255 have implications for application and should especially be considered in cases where the
256 continued presence of viable cells will be required for multiple cycles of precipitation.

257 Considering that the total amount of precipitate was similar in ureolytic and non-ureolytic
258 isolates, we next investigated whether the differences in the speed of precipitation had any
259 effects on the resulting crystals. As an initial observation, the precipitate recovered from
260 ureolytic strains was a much finer powder than that recovered from non-ureolytic strains.
261 EDX analyses of the different precipitates confirmed that all crystals tested were composed
262 of calcium carbonate (Fig. S6). However, further investigation using SEM revealed that the
263 crystal morphology differed between ureolytic and non-ureolytic strains (Fig. 5). When

264 precipitation was rapid, such as in ureolytic strains CG7_3 (Fig.5) and *S. pasteurii* (Fig. S5
265 and Fig S7), inorganic, homogenous crystals were produced. Non-ureolytic strains such as
266 MM1_1 that precipitated calcium carbonate more slowly produced crystals containing
267 significant proportions of bacterial cells and appeared more "organic" in nature (Fig. 5B).
268 Similarly, under these conditions CG4_2 and CG6_1 displayed the gradual increases in pH
269 (Fig. S5) and more organic precipitate characteristic of non-ureolytic strains (Fig. S7).
270 Considering that the assay conditions used for this experiment were high nitrogen, it can be
271 expected that urease activity was repressed under these conditions and resulted in strains
272 behaving like non-ureolytic strains. This differing appearance of precipitates in ureolytic
273 versus non-ureolytic conditions was consistently observed across all isolates tested in this
274 assay (Fig. S5 and Fig. S7). These results show that the differences in ureolytic activity
275 across our environmental isolates not only affected the kinetics of biomineralization, but also
276 had a clear impact on the crystal morphologies in the resulting precipitate.

277 **Profound effects of urease activity on precipitation of calcium carbonate**

278 To exclude that the observed differences in calcium carbonate precipitation were simply due
279 to strain-to-strain variation among our isolates, we exploited the fact that CG7_3 was
280 capable of switching between ureolytic and non-ureolytic states depending on the availability
281 of urea (Fig. 2 and Fig. S3). This allowed us to directly investigate the impact of ureolysis on
282 biomineralization in a single strain. When CG7_3 was grown in the absence of urea, there
283 was a gradual rise in pH and calcium carbonate precipitation as seen in non-ureolytic strains
284 (Fig. 6A). In contrast, in broths supplemented with urea we observed the rapid rise in pH and
285 associated calcium carbonate precipitation characteristic of the ureolytic strains studied
286 above (Fig. 6B). Viable cell counts also dropped dramatically in CG7_3 utilising urea (Fig.
287 6B), whereas in the absence of urea CG7_3 cell numbers remained relatively stable over the
288 first 10 days and declined by 13 days, likely due to prolonged nutrient depletion. SEM
289 analysis of the precipitates over the time-course of the study confirmed our previous
290 observations (Fig. 5) that urease activity was correlated with the rapid precipitation of

291 homogenous, inorganic crystals (Fig. 6B). When assessed over time, we noticed that the
292 initial precipitate consisted of the spherical calcium carbonate, typical of the polymorph
293 vaterite, followed by the eventual conversion into the rhombohedral morphology associated
294 with calcite, the more stable polymorph (Fig. 6B and Fig. S8-S9). In comparison, in the
295 absence of urea CG7_3 precipitated calcium carbonate more gradually, and these
296 precipitates were very organic in appearance (Fig. 6A and Fig. S8-S9). Moreover, these
297 'organic' crystals were often much larger than the inorganic spheres produced in the
298 presence of urea, likely due to aggregation via interspersed bacterial cells. As these
299 experiments were all performed on the same bacterial isolate, our observations are a direct
300 reflection of the effects of urease activity on calcite precipitation. Although both pathways
301 produced similar quantities of precipitate, there were major differences in precipitate
302 morphologies, number of viable bacteria and pH of the bulk phase. To our knowledge, this is
303 the first systematic study into the fundamental differences in biomineralization between
304 different environmental bacteria. Both ureolytic and non-ureolytic bacteria are currently being
305 developed for a range of industrial applications (DeJong *et al.*, 2010). The findings reported
306 here may therefore offer a key step towards a rational design approach to choosing which
307 mechanism of biomineralization is better suited to specific industrial applications.

308

309 **Industrial relevance of different calcite precipitation strategies**

310 To test if the differences in biomineralization mechanism translate to an applied setting, we
311 next assessed the performance of ureolytic and non-ureolytic strains in self-healing concrete
312 applications, using cement mortars as our test system. We produced spores for each strain,
313 which were then encapsulated in light-weight aggregate before casting them in mortars,
314 together with yeast extract and calcium nitrate, as well as urea in the case of ureolytic
315 strains, to provide nutrients for bacterial growth and sufficient calcium for biomineralization.
316 Mortars were cured and then cracked under three-point bending to obtain a target crack
317 width of 500 μM. The self-healing process was subsequently monitored over 8 weeks.

Autogenous healing, which occurs to some degree due to cement hydration, was seen in control mortars that lacked any bacterial spores (Fig. 7 and Fig. 8). This healing was mostly observed along the top edge of the crack and rarely extended down the sides of the mortar prism. Mortars containing either ureolytic or non-ureolytic bacteria also displayed crack healing, and this generally extended across the top as well as down the sides of the crack (Fig. 7 and Fig. 8). However, healing in mortars containing ureolytic bacteria was less regular than seen with non-ureolytic strains, with the sides of cracks not consistently sealing (Fig. 8).

The key aim of bacteria-induced self-healing of concrete is to re-establish water tightness of the structure to prevent water ingress and subsequent corrosion of steel reinforcement. While visual inspection allowed an initial assessment of the healing process, we next sought to test water tightness of our mortars using water flow tests following eight weeks of healing. Recovery of water tightness in mortars containing only the standard cement mix, with no nutrients or additional calcium showed variable recovery of water tightness, generally close to 40 % (Fig. 9, ‘Reference’). Control mortars containing yeast extract and calcium nitrate, but without bacterial spores, showed much higher recovery (averaging 87-95 %). This recovery is likely because of a combination of autogenous healing and possible presence of environmental bacteria, which may be able to utilise the yeast extract and thus contribute to precipitation. As the mortars were not made or kept in a sterile fashion to more closely reflect industrial application, contamination with such environmental bacteria must be considered likely. The mortars containing non-ureolytic bacteria showed a strikingly consistent recovery in water tightness, leading to near complete resistance to water flow, with all specimens healing to over 90 % and many reaching close to 100% (Fig. 9). Interestingly, while mortars containing ureolytic bacteria also showed good restoration of water tightness, there was more variation in the degree of healing obtained. EM1 performed as well as the non-ureolytic strains, but CG7_3 showed lower overall recovery values (mean 87 %) that were similar to the controls lacking encapsulated bacteria. This discrepancy in results may reflect the

variability in ureolytic activity in these strains. Given the clear dependence on growth conditions in some strains described above, it is difficult to predict the degree of ureolytic ability displayed in cement mortars. An alternative explanation may be that the rapid precipitation and small crystal size observed in ureolytic isolates does not reliably lead to retention of the precipitate within the crack and may thus not perform as reliably in self-healing as the larger aggregates with organic components of the non-ureolytic strains. It will be interesting to investigate the details of material performance following healing with both types of bacteria to fully understand the implications of the different mechanisms of precipitation.

CONCLUDING REMARKS

The environment represents a large reservoir of potential in terms of exploiting bacteria for commercial use of MICP. There have been numerous studies on MICP for varying applications, however, most of these have been restricted to the use of a single or small number of species and were very application specific. This limits our understanding of precipitation capabilities of environmental bacteria more generally. In order to establish a stronger knowledge base to facilitate new and specialised technical applications we surveyed the ability of environmental bacteria to precipitate calcite. We found that the majority of isolates were capable of biomineralization, in line with previous results (Boquet *et al.*, 1973). This is most likely due to their ability, through metabolic processes, to create a microenvironment around the cell that aids in the precipitation process. The electronegative nature of their cell surface facilitates crystal deposition on the surface (Schultze-Lam *et al.*, 1996), making precipitation more favourable. Our detailed characterisation of biomineralization by our set of isolates, however, revealed fundamental differences in the way in which different bacteria precipitate calcium carbonate.

370 Ureolytic bacteria rapidly precipitate calcium carbonate, having led to ureolysis becoming
371 one of the main pathways used in MICP applications to date. However, in our study, only 16
372 % of isolates were able to cleave urea, and even amongst these there was a marked
373 diversity in ureolytic activity. Differences in how isolates regulate urease activity were seen,
374 with some responding to low nitrogen levels whilst others responded to urea as a primary
375 inducer. This was in striking contrast to the constitutive high urease activity of *S. pasteuri*,
376 one of the most frequently utilised MICP-capable bacteria to date (Stocks-Fischer *et al.*,
377 1999; Tobler *et al.*, 2011; Zhu *et al.*, 2016). The performance of ureolytic bacteria will
378 therefore depend on the precise conditions encountered in their environment, and this
379 should be carefully considered when choosing the bacterial species for a given application.
380 The importance of this point is further emphasised by our finding that ureolysis affected
381 crystal formation both in terms of kinetics and in the morphology of the precipitate.

382 The majority of our isolates precipitated calcium carbonate without possessing ureolytic
383 activity. In contrast to initial expectations that this mechanism may lead to the formation of
384 low amounts of precipitate, we found that all of our isolates were capable of precipitating the
385 total amount of calcium supplied in the growth media, although this process took more time
386 with non-ureolytic strains. Importantly, we showed that the precipitate formed by the non-
387 ureolytic bacteria consisted of larger, mixed organic/inorganic crystals. This was in good
388 agreement with our initial observation that precipitation in these bacteria on solid media only
389 occurred on top of the colony and therefore likely involved the physical presence of cells.
390 The mixed nature of the precipitate means that for the same amount of calcium being used,
391 a larger volume of precipitate can be formed. This could present a major advantage in
392 industrial application where often only a limited amount of calcium is available to fill a
393 relatively large space, such as in self-healing concrete.

394 When we tested the performance of our isolates in self-healing of cracked cement mortars,
395 we found that, indeed, non-ureolytic bacteria caused a more consistent recovery of water
396 tightness and more complete healing. The ureolytic bacteria tested showed less consistency

397 in performance, although one strain gave similar results to the non-ureolytic isolates. It is
398 difficult to ascertain whether these inconsistencies in behaviour are due to differences in
399 ureolytic activity in the applied setting or are a consequence of the purely inorganic
400 precipitate formed by ureolytic strains. It seems plausible that the supply of yeast extract as
401 part of the cement mix will lead to a low-nitrogen environment conducive to urease gene
402 expression, and the presence of urea should ensure activity in those strains that are urea-
403 responsive. While further experimentation is needed to determine the precise conditions
404 encountered by the bacteria within hardened cement mortars as well as the material
405 properties of the precipitate formed, in applications where nutritional supply is hard to
406 control, the use of non-ureolytic bacteria may give more robust and reliable performance.

407 Self-healing concrete of course only represents one of many potential applications of MICP
408 and each application will have its own challenges. For example, in spray-on applications
409 such as restoration of existing structures and historic buildings, the rapid precipitation of
410 large amounts of precipitate through ureolysis may be advantageous. In contrast, during soil
411 stabilisation where bacteria and their substrates are pumped into the ground, rapid rates of
412 ureolysis could result in premature precipitation and lead to blockages at the injection site as
413 has been reported (Cheng and Cord-Ruwisch, 2014). In this case, it would be more
414 beneficial to use microbes that are non-ureolytic, or that switch to ureolysis at a later time
415 point, as seen in our isolates that responded to low environmental nitrogen.

416 In summary, most bacteria have the ability to precipitate calcium carbonate given the right
417 conditions, and the most suitable bacteria to use will be application dependent. While most
418 previous studies have focussed on one or two isolates, we here show for the first time the
419 plethora of MICP activities and capabilities the environment has to offer as a 'talent pool' that
420 can offer bespoke solutions to many different applications. MICP-based technologies may
421 offer solutions to problems caused by a rising global population and may even be used to
422 mitigate global warming. The increasing demand for infrastructure, as well as the need to
423 engineer land on which to build it, results in an increase in CO_2 emissions and release of

424 harmful chemicals into the environment (DeJong *et al.*, 2010). MICP can reduce this
425 environmental burden by producing buildings that are more durable, prolonging the life of
426 existing buildings, and improving soil properties without the use of toxic and hazardous
427 chemical additives. Moreover, technologies that actively remove CO_2 from the environment
428 and sequestrate it in harmless or even useful minerals such as calcite will be critical in
429 meeting zero emission goals in the future.

430

431 **EXPERIMENTAL PROCEDURES**

432 **Bacterial isolates and growth**

433 Sample collection was from six locations across the United Kingdom including limestone
434 caves and immature calcareous soils (Mendip Hills, England), soil, rock and limestone caves
435 (Bath, England), soil and rock scrapings (Monmouthshire, Wales) and soil and scrapings
436 from marine rock in two locations in Cornwall (Mount's Bay and Falmouth). Samples were
437 stored at 4°C until use. Of each sample, 0.5 g was re-suspended in 1 ml sterile saline
438 solution (0.85% (w/v) NaCl) and heated to 80°C for 20 minutes to enrich for spore-formers.
439 Selection for alkali-tolerant bacteria was carried out by plating 100 µl of this suspension onto
440 0.25× B4 medium (1 g l^{-1} yeast extract, 12 g l^{-1} Trizma base, 1.25 g l^{-1} glucose, 2.5 g l^{-1}
441 calcium acetate ($Ca(OAc)_2$), 15 g l^{-1} agar) adjusted with NaOH to pH 9. Glucose and
442 $Ca(OAc)_2$ were filter-sterilised and added after autoclaving. Individual colonies with unique
443 colony morphology were re-streaked onto 0.25× B4 medium buffered with 75 mM CHES, 75
444 mM CAPS, adjusted with NaOH to pH 10. Strains capable of growth at pH 10 and with
445 visible crystals on the colony or in the surrounding agar were selected for further
446 characterisation. Single colonies were inoculated in lysogeny broth (LB; 10 g l^{-1} tryptone, 5 g
447 l^{-1} yeast extract, 10 g l^{-1} NaCl) and grown overnight, before storage at -80 °C in a 25% (w/v)
448 glycerol solution. Isolates were subsequently maintained on LB agar.
449 *Sporosarcina pasteurii* DSM33 was included as a reference organism and maintained on LB

450 agar supplemented with 20 g l^{-1} urea (filter-sterilized, added after autoclaving). All bacterial
451 cultures were grown at 30 °C, and liquid cultures were agitated at 150 rpm. Growth of liquid
452 cultures was monitored spectrophotometrically by optical density at 600 nm wavelength
453 (OD_{600}) in cuvettes of 1 cm light path length. Representative isolates showing the best
454 characteristics were deposited into the DSMZ collection (Deutsche Sammlung von
455 Mikroorganismen und Zellkulturen GmbH, Germany) as follows*: DSM XX (RC1_1), DSM
456 XX (PD1_1), DSM XX (EM1), DSM XX (CG7_3), DSM XX (CG7_2), DSM XX (CG6_1), DSM
457 XX (CG4_2), and DSM XX (MM1_1).

458 **Note to reviewers: The DSM numbers have not yet been issued but will be available by the*
459 *time the manuscript has been through the review process.*

460

461 **Identification of isolates and phylogenetic analysis**

462 The 16S rDNA gene fragment was amplified using the 27F (5'-
463 AGAGTTTGATCMTGGCTCAG-3') and 1492R (5'-TACCTTGTTACGACTT- 3') primers
464 (Lane, 1991). Amplification was performed in a total volume of 25 µl containing 12.5 µl of 2x
465 OneTaq Mastermix (New England Biolabs, NEB), 9.9 µl of nuclease-free H_2O, 2.4 % (v/v)
466 DMSO, 0.2 µM of each primer and 1 µl of an overnight culture as template. Reaction
467 conditions were as follows: initial denaturation at 94 °C for 5 min followed by 30 cycles
468 consisting of denaturation at 94°C for 30 sec, annealing at 45° C for 30 sec, and extension
469 at 68 °C for 2 min. Final extension was at 68°C for 5 min. For enzymatic clean-up, 2 µl of
470 EXO-SAP (100 U shrimp alkaline phosphatase (Thermo Scientific), 100 U Exonuclease I
471 (Thermo Scientific), and 895 µl nuclease-free H_2O) was added to every 5 µl of PCR product
472 and the reaction was incubated at 37°C for 15 min before enzyme inactivation at 80°C for 15
473 min. Sequencing of PCR products was carried out using the chain termination method
474 (Eurofins Genomics, Germany). In the case of strains where direct sequencing of the PCR
475 product was unsuccessful, 16S rDNA fragments were first cloned into the Topo® vector

476 according to manufacturer's instructions (TOPO TA Cloning® Kit, Invitrogen). Sequencing of
477 the resulting plasmids was performed using the M13 forward primer (5'-
478 CCCAGTCACGACGTTGTAAAACG-3'). Bioedit (Hall, 1999) was used to assemble
479 sequences obtained from forward and reverse sequencing reactions. Sequences were
480 compared against the non-redundant GenBank nucleotide collection using BLASTN
481 (http://www.ncbi.nlm.nih.gov). For phylogenetic analyses, the 16S rDNA sequences of
482 nearest relatives for each strain according to BLASTN analysis, as well as of
483 *Sporosarcina pasteurii* DSM 33 were obtained from GenBank, and evolutionary analyses
484 were carried out in MEGA 7.0 (Kumar *et al.*, 2016). Sequences were aligned using
485 MUSCLE, and conserved blocks were selected from these multiple alignments using
486 GBlocks (Castresana, 2000). Phylogenetic trees were constructed using the maximum
487 likelihood (ML) method based on the Tamura-Nei model (Tamura and Nei, 1993). Bootstrap
488 values were inferred from 1000 replicates and partitions reproduced in less than 50 %
489 bootstrap replicates were collapsed.

490

491 **Analysis of calcium carbonate precipitation**

492 Spatial distribution of calcite precipitation and pH changes was assessed by spotting 20 µl of
493 an overnight culture (OD_{600} adjusted to 1) onto nutrient agar (Oxoid, 23 g l^{-1}) supplemented
494 with phenol red (0.025 g l^{-1}) and $Ca(OAc)_2$ (2.5 g l^{-1} or 10 g l^{-1}), with or without urea (20 g l^{-1}).
495 Physical appearance of plates and crystals were recorded photographically at 1 hr, 3 hr, 5
496 hr, 24 hr, and 48 hr.

497 Rate of mineral precipitation over time was determined by inoculating (1:1000) 150 ml LB
498 broth supplemented with 10 g l^{-1} $Ca(OAc)_2$ from overnight cultures and monitoring viable cell
499 numbers, pH, and insoluble calcium precipitated over time. Viable cells were determined as
500 colony-forming units (CFU) by the plate count method. pH was recorded from aliquots of the
501 culture using a pH electrode (Jenway 924 030, Cole-Parmer, Staffordshire UK) coupled to a

502 pH meter (Jenway 3510 pH Meter). Insoluble precipitate was recovered by centrifugation
503 (975 × *g*, 2 minutes at room temperature (RT)) and washed three times in 50 ml distilled
504 water to remove planktonic cells and culture medium before oven drying at 50 °C for 48
505 hours. Morphology of dried precipitates was examined at accelerating voltages ranging from
506 10 to 20 kV by scanning electron microscopy (SEM; JSM 6480LV, JEOL, Welwyn, UK)
507 equipped with an energy dispersive x-ray (EDX) analyser for elemental analysis.
508 Representative samples were prepared by spreading dried precipitate on double-sided
509 carbon tape placed on aluminium stubs. For EDX, samples were placed under vacuum
510 overnight before analysis. For imaging, samples were gold-coated by sputtering for 3 min at
511 RT. Samples imaged with field emission electron microscopy (FE-SEM; JSM-6301F cold
512 field emission SEM, JEOL) were prepared in a similar manner as for SEM but coated in
513 Chromium to a thickness of 20 nM and examined at 5 kV.

514

515 **Urease activity**

516 Qualitative urease activity of bacterial isolates was determined using urease test broth (0.1 g
517 l^{-1} yeast extract, 20 g l^{-1} urea, 0.01 g l^{-1} phenol red, 0.67 mM KH_2PO_4, 0.67 mM Na_2HPO_4 (pH
518 6.8±0.2). Test broth (2 ml) was inoculated with 100 µl of an overnight culture grown in LB
519 and incubated at 30 °C for up to 5 days. A urease-positive reaction was characterised by a
520 change in colour from yellow/orange to pink.

521 For quantitative urease measurements in whole cells, cultures were grown at 30 °C with
522 agitation (150 rpm). Overnight cultures (20 µl, LB broth) were used to inoculate 25 ml (1:500)
523 low nitrogen (0.2 g l^{-1} yeast extract, 0.125 g l^{-1} peptone, 2.5 g l^{-1} NaCl) and standard media
524 (2 g l^{-1} yeast extract, 1.25 g l^{-1} peptone, 2.5 g l^{-1} NaCl) broths. Where pre-induction by urea
525 was required, broths were supplemented with urea (20 g l^{-1}). Cultures were grown (for 24 hr)
526 and cells were harvested from 1 ml of culture by centrifugation (8000 *x g*, 2 min). Cells were
527 resuspended in 1 volume 0.1 M potassium phosphate buffer (pH 8.0), and OD_{600} was

528 recorded. Depending on the urease activities of individual strains, dilutions of cells were
529 made to ensure the activity was within the linear range of the assay. These dilutions were
530 recorded and accounted for during OD normalisation. Urease activity was determined
531 according to the phenol-hypochlorite method (Natarajan, 1995) and adapted from (Achal *et*
532 *al.*, 2009) for whole cells. The reaction mix volumes were multiplied by the number of time-
533 points in the assay to allow one larger volume mix to be prepared. Per time point, individual
534 reactions contained 75 µl cell suspension, 300 µl 0.1 M potassium phosphate buffer (pH 8.0)
535 and 750 µl 0.1 M urea solution. The mixture was incubated at 30°C and 1 ml aliquots were
536 removed at 0, 30, 60, 90 and 120 min. At each time point, the reaction was stopped by
537 adding 300 µl phenol nitroprusside and 300 µl alkaline hypochlorite. Final colour was
538 developed at 37 °C for 25 min and absorbance was measured at 625 nm. Ammonium
539 chloride (25-2500 µM) solutions were used to produce a standard curve (Fig. S1). One unit
540 of activity was defined as the release of 1 µM of ammonia per minute, per OD (U OD^{-1} ml^{-1}).

541

542 **Endospore production**

543 Endospores of bacterial strains were prepared by inoculating 150 ml LB broth (1:1000) from
544 an overnight culture grown at 30°C with shaking (150 rpm). This culture was again grown
545 overnight and then cells were harvested by centrifugation (3200 × *g*, 10 min at RT) and
546 resuspended in 750 ml Difco sporulation medium (DSM; 8 g l^{-1} nutrient broth (Oxoid), 13.41
547 mM KCl, 0.49 mM $MgSO_4$, adjusted to pH 7.6 with NaOH. Prior to use 1mM $Ca(NO_3)_2$, 0.01
548 mM $MnCl_2$, and 1µM $FeSO_4$ were added from a filter-sterilised stock solution (Sonenshein *et*
549 *al.*, 1974). Cultures were grown with agitation (150 rpm) at 30 °C for at least 48 hours before
550 sporulation was assessed using phase contrast microscopy. When the majority of cells
551 contained phase-bright endospores, cells were pelleted by centrifugation (3200 × *g*, 10 min
552 at RT) and washed thrice in 10 mM Tris-HCl (pH 9) followed by 30 min treatment with
553 chlorohexidine digluconate (0.3 mg ml^{-1}) to kill vegetative cells. Washing was repeated as

before and spore pellets were snap-frozen in liquid nitrogen and freeze-dried under vacuum overnight.

Preparation of mortar samples

Mortar prisms (65 mm × 40 mm × 40 mm) were comprised of two layers. The first contained (per 3 prisms): 253.3 g sand conforming to BS EN 196-1, 92 g Portland limestone cement (CEM II A-L 32.5R), 46 g water, 1 g yeast extract, 4.55 g calcium nitrate, 3.54 g aerated concrete granules. Mortars containing ureolytic bacteria also contained urea (3.68 g per 3 prisms). Spores (2.1 x 10^{10} cfu) were resuspended in 1 ml dH_2O and imbibed into the aerated concrete granules before drying and sealing with polyvinyl acetate (PVA, 30% (w/w)). After approximately 3 hours, the second, top layer was cast. The second layer contained standard cement mortar (Per 3 prisms: 276g standard sand, 92 g cement, 46 g water). Reference specimens were cast in two layers but only contained standard cement mortar. Specimens remained at room temperature for 24-48 hours before demoulding and subsequent curing for 28 days submersed in tap water. After curing, specimens were oven dried at 50 °C for 24 hours. The top third of the prism was wrapped with carbon fibre reinforced polymer strips to enable generation of a crack of controlled width. A notch (1.5 mm deep) was sawn at mid-span to serve as a crack initiation point. Specimens were cracked by three-point bending using a 30 kN Instron static testing frame. A crack mouth opening displacement (CMOD) gauge was used to measurement crack width. Load was applied to maintain a crack growth of 25 µm per minute, and loading was stopped when the crack width was predicted to be 500 µm wide after load removal. A marker pen was used to indicate specific crack sections to enable monitoring of the crack at the same site. Following cracking, prisms were placed in tanks, open to the atmosphere and filled with tap water to 1 cm below the top of the mortars, and were incubated at room temperature for two months. Visualisation of crack healing was monitored using a Leica M205C light microscope, and images were taken of freshly cracked mortars and after 1, 4, and 8 weeks of healing.

Water permeability tests

Water flow rate before cracking, after cracking, and after 8 weeks of healing was determined to monitor effects of cracking and healing on water permeability in mortars as described previously (Lee and Ryou, 2016). The instrument used was based on RILEM test method II.4 (RILEM, 1987). The bottom of a 10 ml measuring cylinder (0.2 ml graduation) was removed and a 40 mm PVC pipe with 15 mm depth was fixed to the bottom. This was sealed onto the mortar with glue. This cylinder was filled with water and the time it took to drop from initial height h_1 to a final height h_2 was recorded. The total height was either 78.5 mm or, in the case of samples with low permeability, the height to which the water level had dropped after 30 min. The permeability coefficient was calculated according to Equation 3 (Lee and Ryou, 2016).

$$k = \frac{aL}{At} ln\left[\frac{h_1}{h_2}\right], \quad (3)$$

where k = water permeability coefficient (cm/s); a = cross-sectional area of the cylinder (1.77 cm^2); L = thickness of specimen (4 cm); A = cross-sectional area of the specimen which equals the cross-sectional area of acrylic plate (10.18 cm^2); t = time (s); h_1 = initial water head (12.4 cm); h_2 = final water head (cm). The percentage of crack healing was calculated as follows:

$$\text{Healing percentage } (\%) = \frac{(k_0 - k_t)}{k_0} \text{ x } 100 \quad (4)$$

where k_0 = initial water permeability after cracking, k_t = water permeability at healing time t.

ACKNOWLEDGEMENTS

The authors would like to acknowledge the Engineering and Physical Sciences Research Council (EPSRC; EP/PO2081X/1) and industrial collaborators/partners for funding the

605 Resilient Materials for Life (RM4L) project. TDH was supported by a University of Bath
606 Research Studentship Award. We thank technical staff in the Department of Architecture and
607 Civil Engineering and the Department of Biology and Biochemistry for key support. We
608 further thank Dr Philip Fletcher and Diane Lednitzky of the Material and Chemical
609 Characterisation Facility (MC^2) at University of Bath (https://doi.org/10.15125/mx6j-3r54) for
610 their assistance with microscopy.

611

612 **REFERENCES**

613 Achal, V., Mukherjee, A., Basu, P.C., and Reddy, M.S. (2009) Lactose mother liquor as an
614 alternative nutrient source for microbial concrete production by *Sporosarcina pasteurii*.
615 *J Ind Microbiol Biotechnol* **36**: 433–438.

616 Achal, V., Pan, X., and Zhang, D. (2011) Remediation of copper-contaminated soil by
617 *Kocuria flava* CR1 , based on microbially induced calcite precipitation. *Ecol Eng* **37**:
618 1601–1605.

619 Alazhari, M., Sharma, T., Heath, A., Cooper, R., and Paine, K. (2018) Application of
620 expanded perlite encapsulated bacteria and growth media for self-healing concrete.
621 *Constr Build Mater* **160**: 610–619.

622 Altermann, W., Kazmierczak, J., Oren, A., and Wright, D.T. (2006) Cyanobacterial
623 calcification and its rock-building potential during 3.5 billion years of Earth history.
624 *Geobiology* **4**: 147–166.

625 Bang, S.S., Lippert, J.J., Yerra, U., Mulukutla, S., and Ramakrishnan, V. (2010) Microbial
626 calcite , a bio-based smart nanomaterial in concrete remediation. *Int J Smart Nano*
627 *Mater* **1**: 28–39.

628 Boquet, E., Boronat, A., and Ramos-Cormenzana, A. (1973) Production of Calcite (Calcium
629 Carbonate) Crystals by Soil Bacteria is a General Phenomenon. *Nature* **246**: 527–529.

630 Castresana, J. (2000) Selection of Conserved Blocks from Multiple Alignments for Their Use
631 in Phylogenetic Analysis. *Mol Biol Evol* **17**: 540–552.

632 Ceci, A., Pinzari, F., Riccardi, C., Maggi, O., Pierro, L., Papini, M.P., et al. (2018) Metabolic
633 synergies in the biotransformation of organic and metallic toxic compounds by a
634 saprotrophic soil fungus. *Environ Biotechnol* **102**: 1019–1033.

635 Cheng, L. and Cord-Ruwisch, R. (2014) Upscaling Effects of Soil Improvement by
636 Microbially Induced Calcite Precipitation by Surface Percolation. *Geomicrobiol J* **31**:
637 396–406.

638 DeJong, J.T., Mortensen, B.M., Martinez, B.C., and Nelson, D.C. (2010) Bio-mediated soil
639 improvement. *Ecol Eng* **36**: 197–210.

640 Hall, T. (1999) Bioedit: a user-friendly biological sequence alignment editor and analysis
641 program for Windows 95/98/NT. *Nucleic Acids Symp Ser* **41**: 95–98.

642 Hammes, F. and Verstraete, W. (2002) Key roles of pH and calcium metabolism in microbial

643 carbonate precipitation. *Rev Environ Sci Biotechnol* **1**: 3–7.

644 Huntzinger, D.N. and Eatmon, T.D. (2009) A life-cycle assessment of Portland cement
645 manufacturing : comparing the traditional process with alternative technologies. *J Clean*
646 *Prod* **17**: 668–675.

647 Jonkers, H.M., Thijssen, A., Muyzer, G., Copuroglu, O., and Schlangen, E. (2010)
648 Application of bacteria as self-healing agent for the development of sustainable
649 concrete. *Ecol Eng* **36**: 230–235.

650 Kumar, S., Stecher, G., and Tamura, K. (2016) MEGA7 : Molecular Evolutionary Genetics
651 Analysis Version 7 . 0 for Bigger Datasets Brief communication. *Mol Biol Evol* **33**:
652 1870–1874.

653 Lane, D. (1991) 16S/23S rRNA sequencing. In, Stackebrandt,E. and Goodfellow,M. (eds),
654 *Nucleic acid techniques in bacterial systematics*. John Wiley and Sons, pp. 115–175.

655 Lee, Y.S. and Ryou, J.S. (2016) Crack healing performance of PVA-coated granules made
656 of cement, CSA, and Na2CO3 in the cement matrix. *Materials (Basel)* **9**: 555–575.

657 Mitchell, A.C., Dideriksen, K., Spangler, L.H., Cunningham, A.B., and Gerlach, R. (2010)
658 Microbially Enhanced Carbon Capture and Storage by Mineral-Trapping and Solubility-
659 Trapping. *Environ Sci Technol* **44**: 5270–5276.

660 Mobley, H.L.T. and Hausinger, R.P. (1989) Microbial Ureases : Significance , Regulation ,
661 and Molecular Characterization. *Microbiol Rev* **53**: 85–108.

662 Natarajan, K.R. (1995) Kinetic Study of the Enzyme Urease from Dolichos biflorus. *J Chem*
663 *Educ* **72**: 556–557.

664 Power, I.M., Wilson, S.A., Small, D.P., Dipple, G.M., Wan, W., and Southam, G. (2011)
665 Microbially Mediated Mineral Carbonation : Roles of Phototrophy and Heterotrophy.
666 *Environ Sci Technol* **45**: 9061–9068.

667 RILEM (1987) Measurement of Water Absorption Under Low Pressure. RILEM Test Method
668 No. 11.4.

669 Schultze-Lam, S., Fortin, D., Davis, B.S., and Beveridge, T.J. (1996) Mineralization of
670 bacterial surfaces. *Chem Geol* **132**: 171–181.

671 Sharma, T.K., Alazhari, M., Heath, A., Paine, K., and Cooper, R.M. (2017) Alkaliphilic
672 *Bacillus* species show potential application in concrete crack repair by virtue of rapid
673 spore production and germination then extracellular calcite formation. *J Appl Microbiol*
674 **122**: 1233–1244.

675 Sonenshein, A.L., Cami, B., Brevet, J., and Cote, R. (1974) Isolation and Characterization of
676 Rifampin-Resistant and Streptolydigin-Resistant Mutants of *Bacillus subtilis* with Altered
677 Sporulation Properties. *J Bacteriol* **120**: 253–265.

678 Souto-Martinez, A., Arehart, J.H., and Srubar III, W. V (2018) Energy & Buildings Cradle-to-
679 gate CO_2 emissions vs . *in situ* CO_2 sequestration of structural concrete elements.
680 *Energy Build* **167**: 301–311.

681 Stocks-Fischer, S., Galinat, J.K., and Bang, S.S. (1999) Microbiological precipitation of
682 $CaCO_3$. *Soil Biol Biochem* **31**: 1563–1571.

683 Tamura, K. and Nei, M. (1993) Estimation of the Number of Nucleotide Substitutions in the
684 Control Region of Mitochondrial DNA in Humans and. *Mol Biol Evol* **10**: 512–526.

685 Tobler, D.J., Cuthbert, M.O., Greswell, R.B., Riley, M.S., Renshaw, J.C., Handley-Sidhu, S.,
686 and Phoenix, V.R. (2011) Comparison of rates of ureolysis between *Sporosarcina*

687 *pasteurii* and an indigenous groundwater community under conditions required to
688 precipitate large volumes of calcite. *Geochim Cosmochim Acta* **75**: 3290–3301.

689 Wang, J., De Belie, N., and Verstraete, W. (2012) Diatomaceous earth as a protective
690 vehicle for bacteria applied for self-healing concrete. *Biotechnol Methods* **39**: 567–577.

691 Wang, J., Jonkers, H.M., Boon, N., and De Belie, N. (2017) *Bacillus sphaericus* LMG 22257
692 is physiologically suitable for self-healing concrete. *Appl Microbiol Biotechnol* **101**:
693 5101–5114.

694 Wilmeth, D.T., Johnson, H.A., Stamps, B.W., Berelson, W.M., Stevenson, B.S., Nunn, H.S.,
695 et al. (2018) Environmental and Biological Influences on Carbonate Precipitation Within
696 Hot Spring Microbial Mats in Little Hot Creek, CA. *Front Microbiol* **9**: 1–13.

697 Zhao, Q., Li, L., Asce, M., Li, C., Li, M., Amini, F., et al. (2014) Factors Affecting
698 Improvement of Engineering Properties of MICP-Treated Soil Catalyzed by Bacteria
699 and Urease. *J Mater Civ Eng* **26**: 1–10.

700 Zhu, T., Dittrich, M., and Dittrich, M. (2016) Carbonate Precipitation through Microbial
701 Activities in Natural environment , and Their Potential in Biotechnology : A Review.
702 *Front Bioeng Biotechnol* **4**: 1–21.

703

704 **FIGURE LEGENDS**

705 **Figure 1. Phylogenetic analysis of selected calcite-precipitating isolates and their**
706 **closest relatives.** Yellow boxes, non-ureolytic isolates; orange boxes, isolates with inducible
707 ureolytic activity; pink boxes, isolates that utilize urea as a primary nitrogen source; unfilled
708 boxes, unknown ureolytic ability. The ureolytic potential of closest relatives is not shown.
709 Accession numbers are indicated in parentheses. The percentage of trees in which
710 associated taxa clustered together is shown next to the branches (1000 bootstraps).

711 **Figure 2. Diversity in ureolytic activity across environmental isolates.** *Left*, urease test
712 broth inoculated with the strains indicated to the left. *Right*, nutrient agar plates
713 supplemented with phenol red, calcium acetate, and urea were inoculated in the centre with
714 suspensions of the same strains. Pink shading indicates the pH change caused by ammonia
715 release from ureolytic activity.

716 **Figure 3. Crystal formation correlates with pH changes in non-ureolytic and ureolytic**
717 **bacteria.** (A) Non-ureolytic isolate PD1_1 shows localised crystals on the bacterial colony.
718 (B) Ureolytic *S. pasteurii* demonstrates crystal precipitation throughout the media,

719 corresponding to pH changes that occur throughout the media. Arrows indicate $CaCO_3$
720 crystals.

721 **Figure 4. Regulation of urease activity by environmental nitrogen and urea.** Isolates
722 CG6_1 (A) and CG7_3 (B) cells were grown in high or low nitrogen conditions in the
723 presence (+) or absence (-) of urea. Error bars represent standard deviation from 2-3
724 biological reps with 1-2 technical reps each. Significance was tested using an unpaired t-test
725 (A) and one-way ANOVA followed by unpaired t-test (B). *, P <0.05, ***, P <0.001 and ****, P
726 <0.0001.

727 **Figure 5. Calcite precipitation kinetics and crystal morphology in ureolytic CG7_3 and**
728 **non-ureolytic MM1_1.** The ureolytic strain CG7_3 (A) and the non-ureolytic MM1_1 (B)
729 were grown in LB medium supplemented with urea (20 g l^{-1}) and $Ca(OAc)_2$ (10 g l^{-1}) and
730 precipitation of insoluble calcium carbonate (bars, g l^{-1}), pH changes (circles) and changes in
731 cell number (boxes, CFU ml^{-1}) were monitored over time (days). Maximum theoretical level
732 of precipitation is indicated (dotted line). *Right,* electron micrographs of representative
733 precipitate taken at day 9.

734 **Figure 6. Comparison of ureolytic and non-ureolytic mechanisms of calcite**
735 **precipitation in CG7_3.** The ureolytic strain CG7_3 was grown in LB medium
736 supplemented with $Ca(OAc)_2$ (10 g l^{-1}) in the absence (A) and presence (B) of urea (20 g l^{-1}).
737 Precipitation of insoluble calcium carbonate (bars, g l^{-1}), pH changes (circles) and changes
738 in cell number (boxes, CFU ml^{-1}) were monitored over time (days). Maximum theoretical
739 level of precipitation is indicated (dotted line). *Right,* electron micrographs of representative
740 precipitate taken at days 3 and 13.

741 **Figure 7. Crack closure in control mortars and mortars containing non-ureolytic**
742 **bacteria.** Cracks in mortar specimens are shown immediately post-cracking and after 8
743 weeks of healing. Cracks were marked with black pen to allow the same region to be
744 monitored over time. Two independent regions along the top of the mortar were monitored

per sample. Side views show the cracks down both sides of the mortar at 8 weeks. *White arrows*, complete crack closure. *Black arrows*, incomplete crack closure.

Figure 8. Crack closure in control mortars and mortars containing ureolytic bacteria. Cracks in mortar specimens are shown immediately post-cracking and after 8 weeks of healing. Cracks were marked with black pen to allow the same region to be monitored over time. Two independent regions along the top of the mortar were monitored per sample. Side views show the cracks down both sides of the mortar at 8 weeks. *White arrows*, complete crack closure. *Black arrows*, incomplete crack closure.

Figure 9. Recovery of water tightness in mortars after two months of bacteria-based self-healing. Water flow through mortars containing ureolytic (CG7_3, EM1) or non-ureolytic (MM1_1, RC1_1) bacteria was determined immediately after cracking and following 8 weeks of healing. Reference mortars contained no additives; Control mortars contained yeast extract and calcium nitrate, but no bacteria. Recovery of water tightness was determined as a percentage relative to the freshly cracked specimen (0%: no change in water flow, 100%: complete inhibition of water flow). Data is shown for four specimens per condition from two separate cracking/healing experiments.

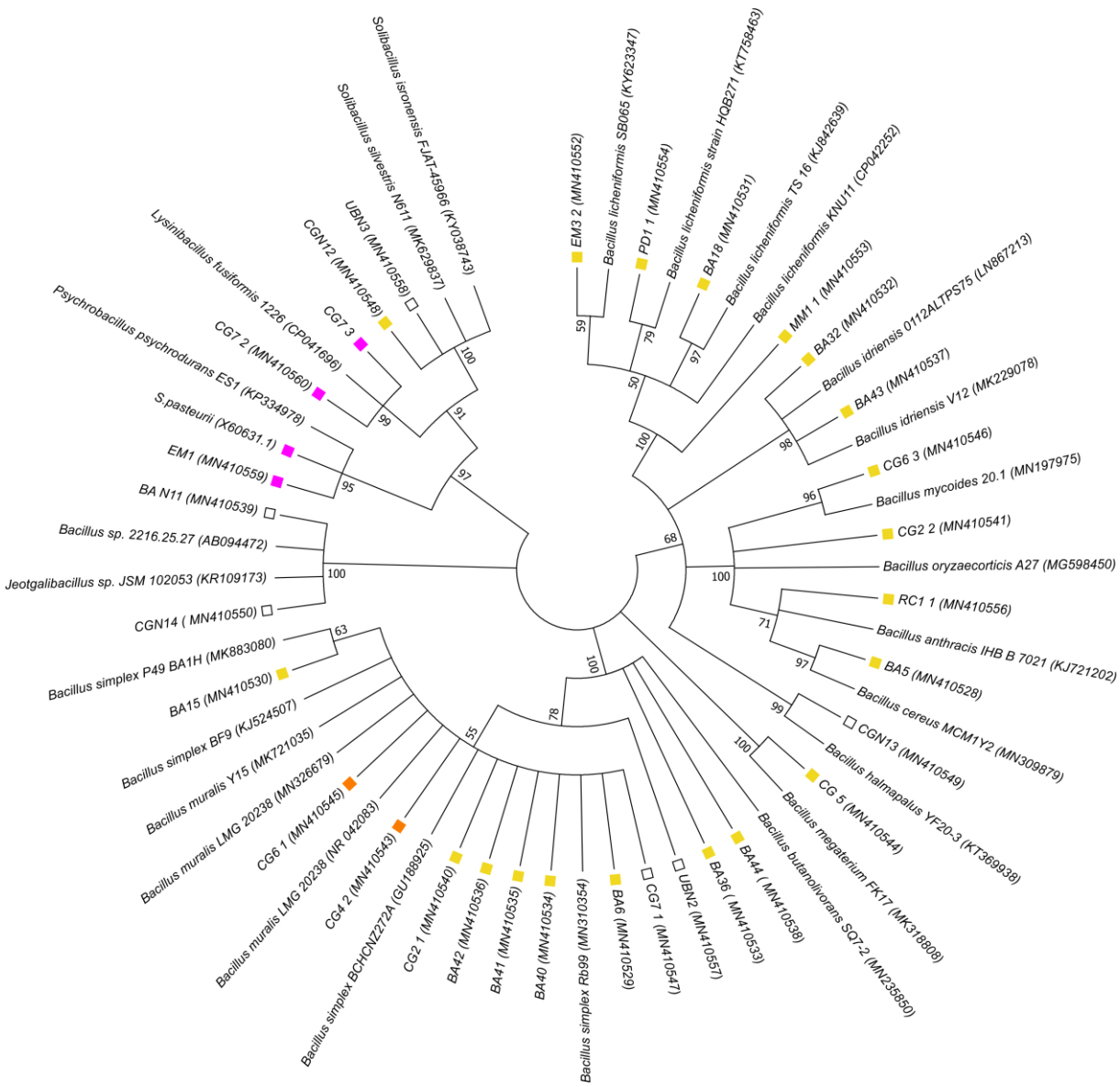

Figure 1. Phylogenetic analysis of selected calcite-precipitating isolates and their closest relatives. Yellow boxes, non-ureolytic isolates; orange boxes, isolates with inducible ureolytic activity; pink boxes, isolates that utilize urea as a primary nitrogen source; unfilled boxes, unknown ureolytic ability. The ureolytic potential of closest relatives is not shown. Accession numbers are indicated in parentheses. The percentage of trees in which associated taxa clustered together is shown next to the branches (1000 bootstraps).

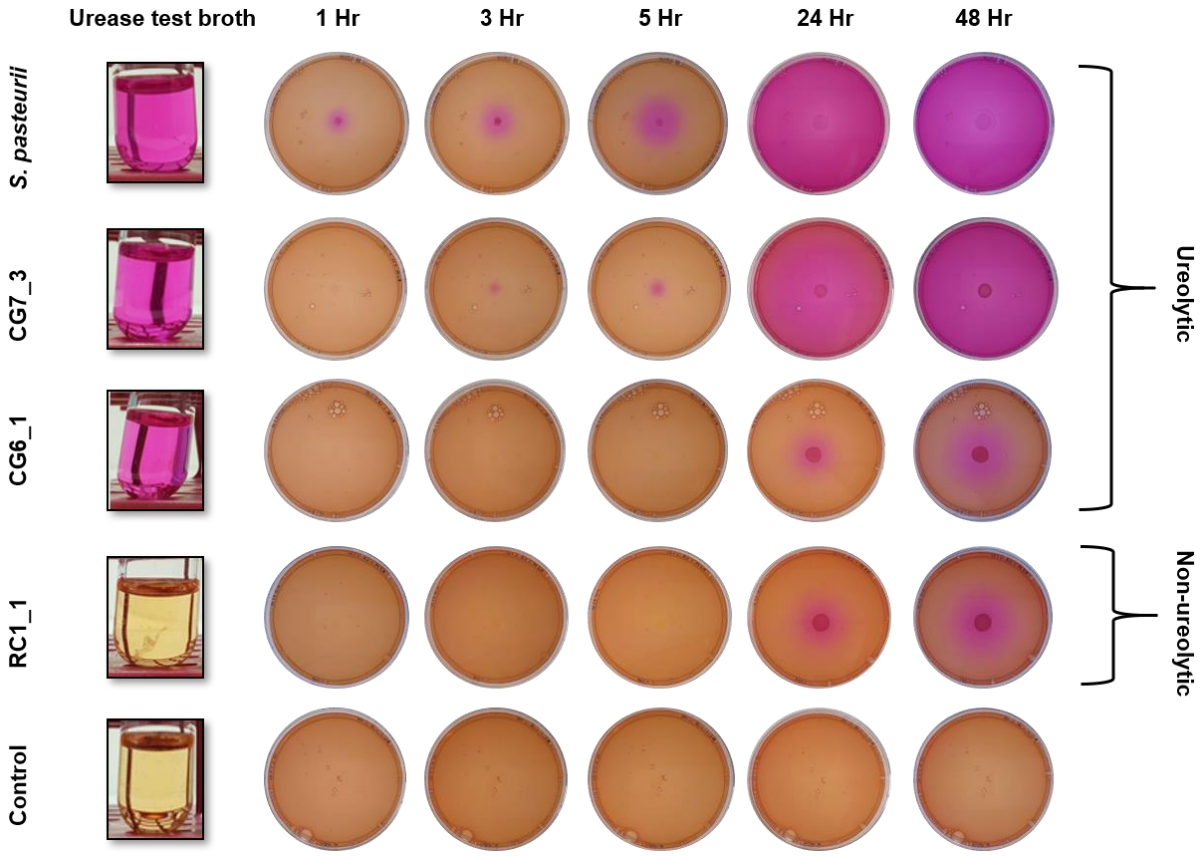

Figure 2. Diversity in ureolytic activity across environmental isolates. *Left*, urease test broth inoculated with the strains indicated to the left. *Right*, nutrient agar plates supplemented with phenol red, calcium acetate, and urea were inoculated in the centre with suspensions of the same strains. Pink shading indicates the pH change caused by ammonia release from ureolytic activity.

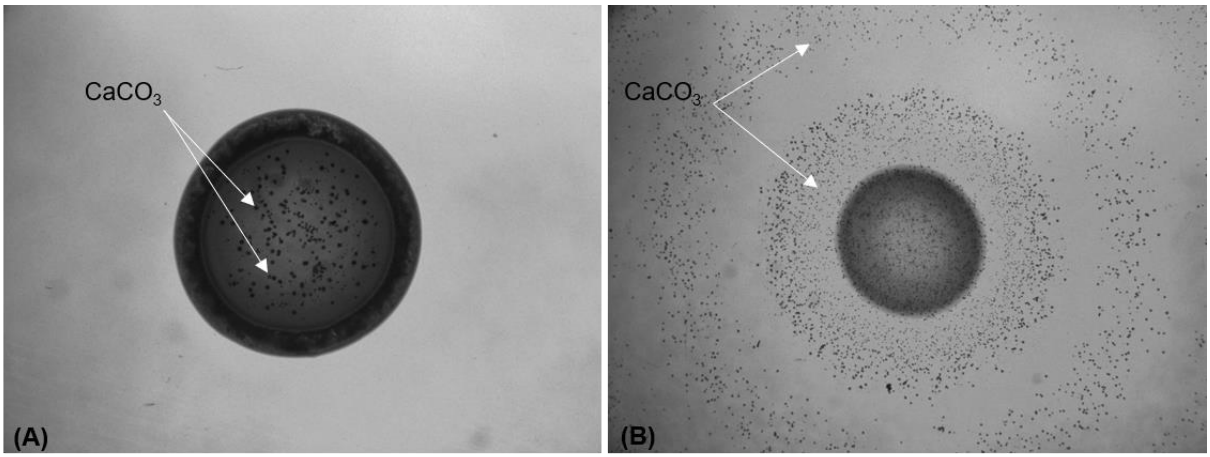

Figure 3. Crystal formation correlates with pH changes in non-ureolytic and ureolytic bacteria. (A) Non-ureolytic isolate PD1_1 shows localised crystals on the bacterial colony. (B) Ureolytic *S. pasteurii* demonstrates crystal precipitation throughout the media, corresponding to pH changes that occur throughout the media. Arrows indicate $CaCO_3$ crystals.

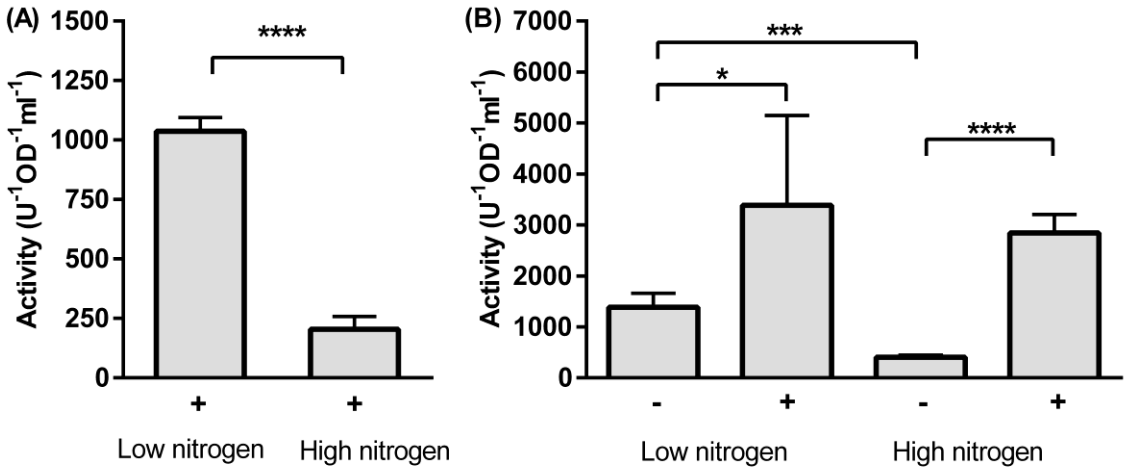

Figure 4. Regulation of urease activity by environmental nitrogen and urea. Isolates CG6_1 (A) and CG7_3 (B) cells were grown in high or low nitrogen conditions in the presence (+) or absence (-) of urea. Error bars represent standard deviation from 2-3 biological reps with 1-2 technical reps each. Significance was tested using an unpaired t-test (A) and one-way ANOVA followed by unpaired t-test (B). *, P <0.05, ***, P <0.001 and ****, P <0.0001.

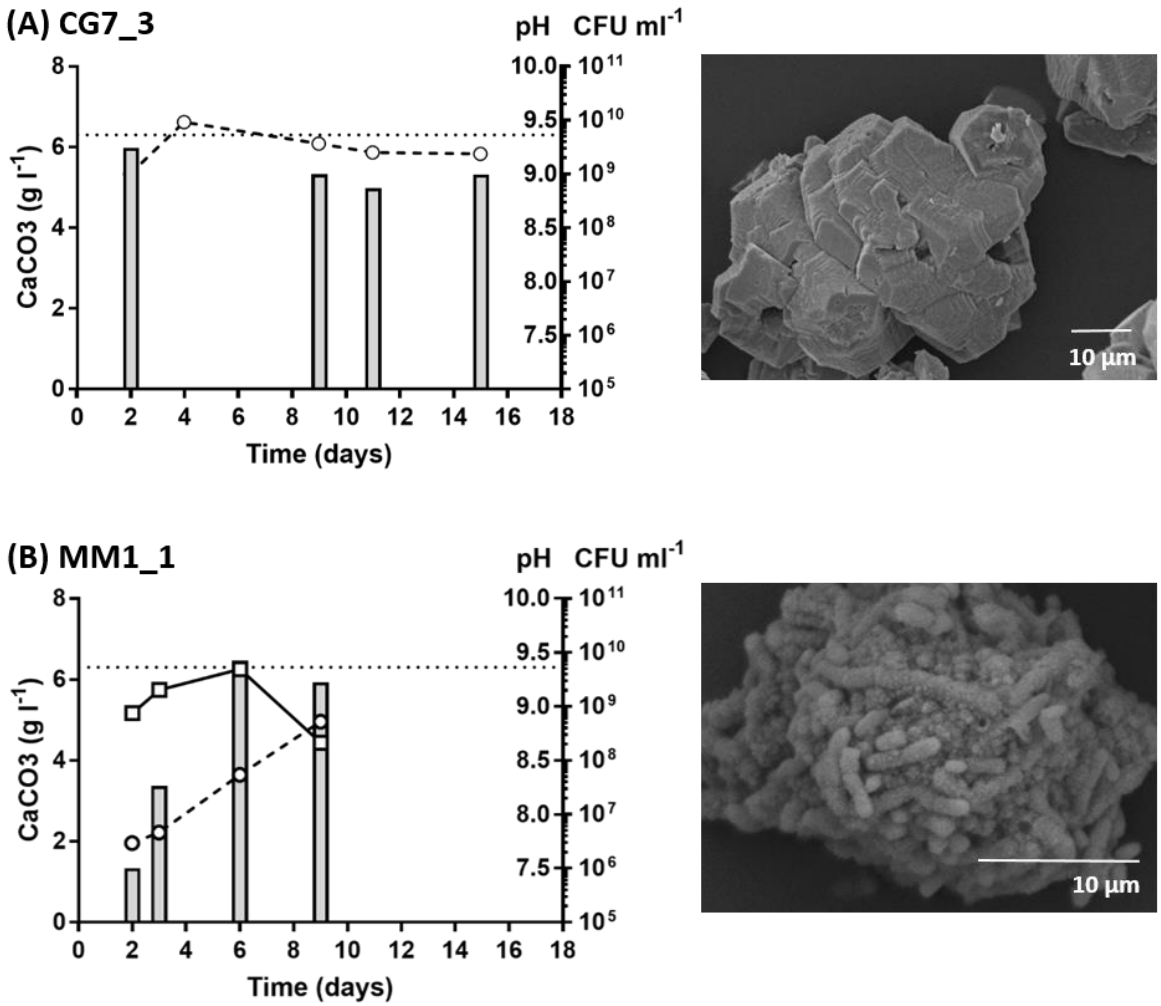

Figure 5. Calcite precipitation kinetics and crystal morphology in ureolytic CG7_3 and non-ureolytic MM1_1. The ureolytic strain CG7_3 (A) and the non-ureolytic MM1_1 (B) were grown in LB medium supplemented with urea (20 g l^{-1}) and $Ca(OAc)_2$ (10 g l^{-1}) and precipitation of insoluble calcium carbonate (bars, g l^{-1}), pH changes (circles) and changes in cell number (boxes, CFU ml^{-1}) were monitored over time (days). Maximum theoretical level of precipitation is indicated (dotted line). *Right,* electron micrographs of representative precipitate taken at day 9.

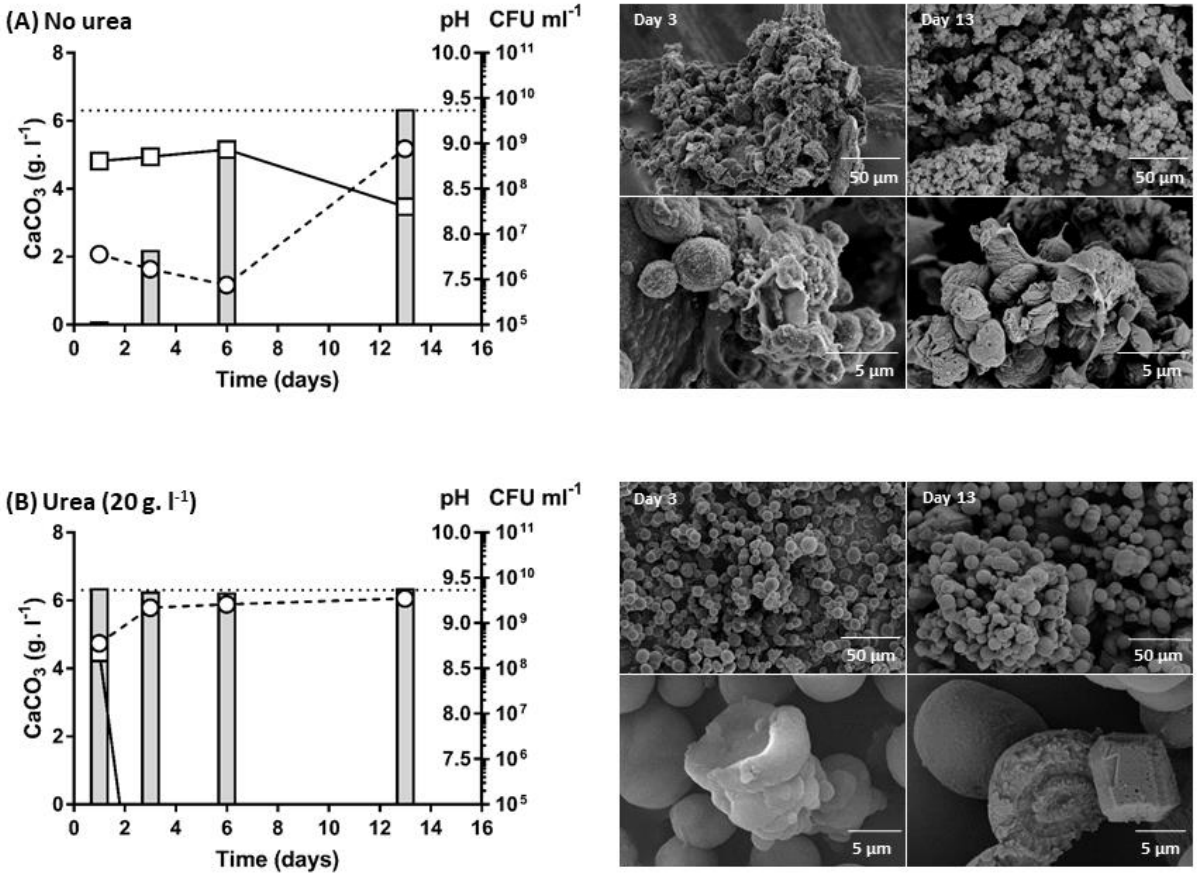

Figure 6. Comparison of ureolytic and non-ureolytic mechanisms of calcite precipitation in CG7_3. The ureolytic strain CG7_3 was grown in LB medium supplemented with $Ca(OAc)_2$ (10 g l^{-1}) in the absence (A) and presence (B) of urea (20 g l^{-1}). Precipitation of insoluble calcium carbonate (bars, g l^{-1}), pH changes (circles) and changes in cell number (boxes, CFU ml^{-1}) were monitored over time (days). Maximum theoretical level of precipitation is indicated (dotted line). *Right,* electron micrographs of representative precipitate taken at days 3 and 13.

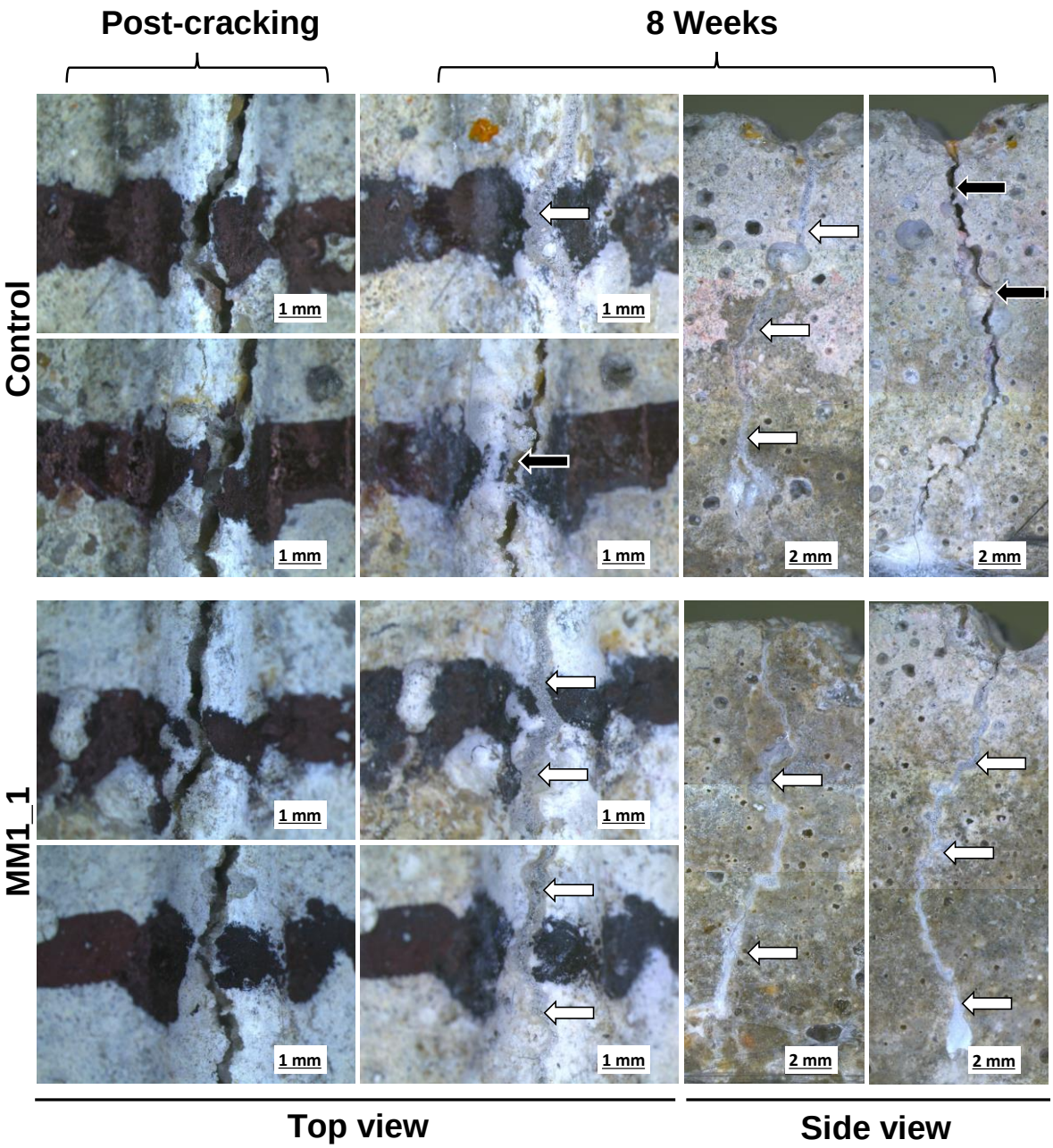

Figure 7. Crack closure in control mortars and mortars containing non-ureolytic bacteria. Cracks in mortar specimens are shown immediately post-cracking and after 8 weeks of healing. Cracks were marked with black pen to allow the same region to be monitored over time. Two independent regions along the top of the mortar were monitored per sample. Side views show the cracks down both sides of the mortar at 8 weeks. *White arrows*, complete crack closure. *Black arrows*, incomplete crack closure.

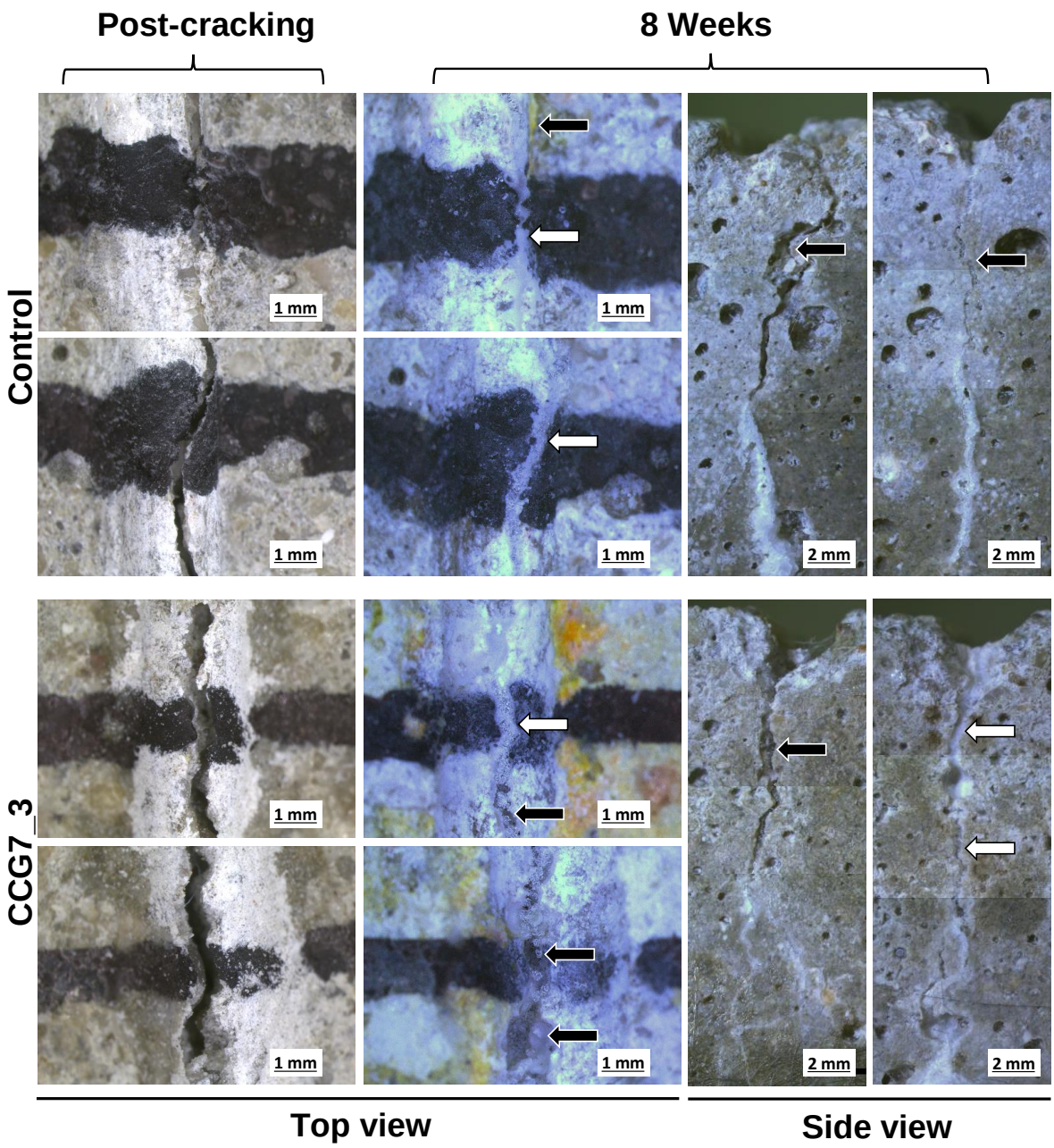

Figure 8. Crack closure in control mortars and mortars containing ureolytic bacteria. Cracks in mortar specimens are shown immediately post-cracking and after 8 weeks of healing. Cracks were marked with black pen to allow the same region to be monitored over time. Two independent regions along the top of the mortar were monitored per sample. Side views show the cracks down both sides of the mortar at 8 weeks. *White arrows*, complete crack closure. *Black arrows*, incomplete crack closure.

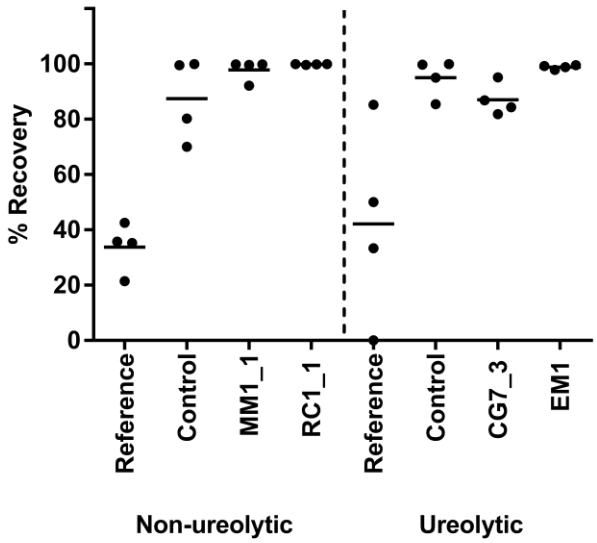

Figure 9. Recovery of water tightness in mortars after two months of bacteria-based self-healing. Water flow through mortars containing ureolytic (CG7_3, EM1) or non-ureolytic (MM1_1, RC1_1) bacteria was determined immediately after cracking and following 8 weeks of healing. Reference mortars contained no additives; Control mortars contained yeast extract and calcium nitrate, but no bacteria. Recovery of water tightness was determined as a percentage relative to the freshly cracked specimen (0%: no change in water flow, 100%: complete inhibition of water flow). Data is shown for four specimens per condition from two separate cracking/healing experiments.

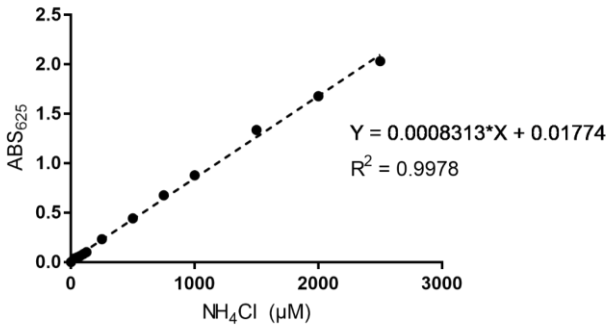

Figure S1. Ammonium chloride concentration vs absorbance standard curve. Ammonium chloride (25-2500 µM) solutions were used as standards to quantify the change in absorbance at 625 nm wavelength (A_{625}) observed using phenol-hypochlorite as described in methods. The linear fit of ammonium chloride concentration versus absorbance used to calculate unknown concentrations is shown by the equation and dashed line.

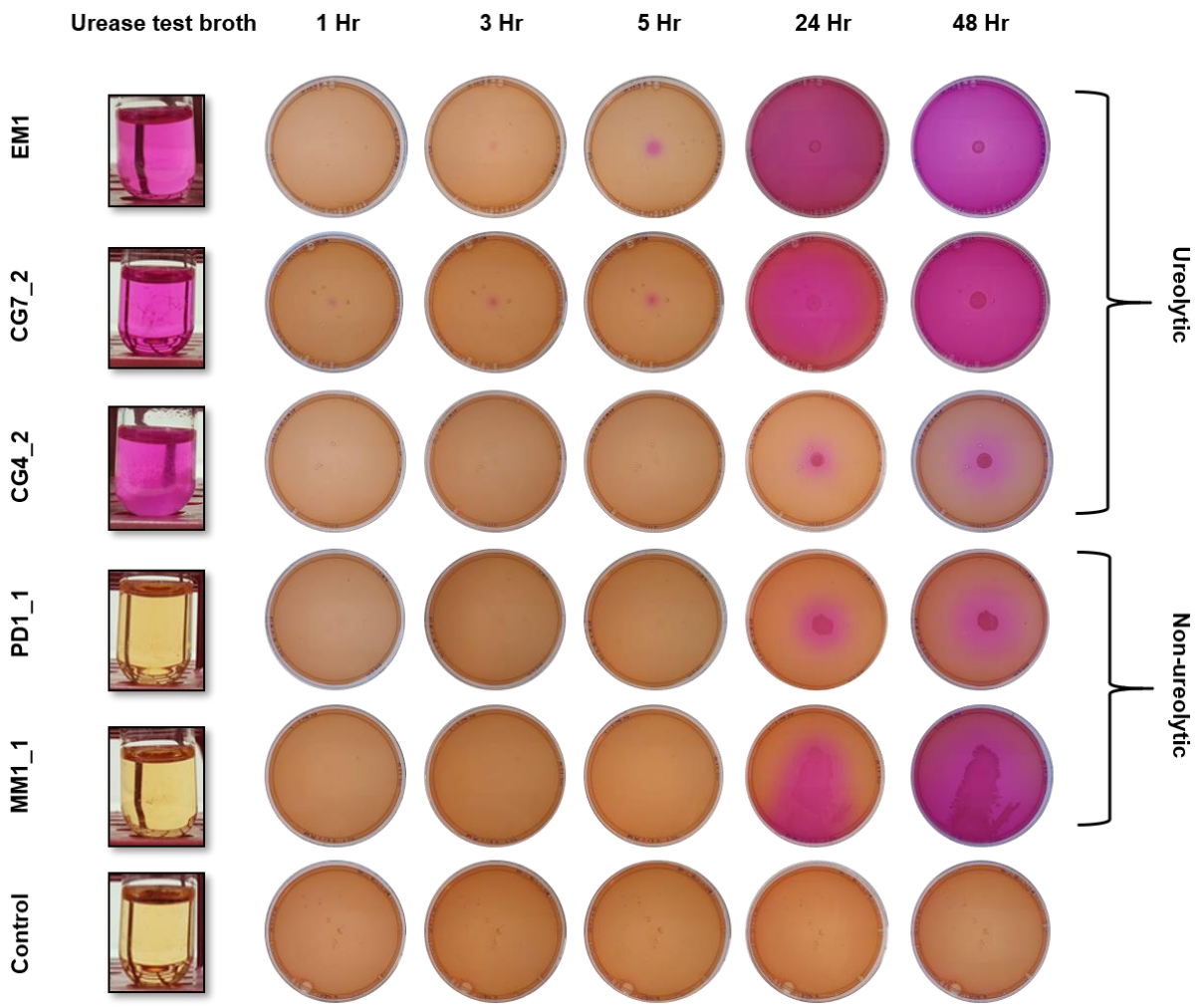

Figure S2. Diversity in ureolytic activity across environmental isolates. *Left*, urease test broth inoculated with the strains indicated to the left. *Right*, nutrient agar plates supplemented with phenol red, calcium acetate, and urea were inoculated in the centre with suspensions of the same strains. Pink shading indicates the pH change caused by ammonia release from ureolytic activity. MM1_1, although non-ureolytic, caused changes in pH likely due to a stress response to urea which resulted in swarming.

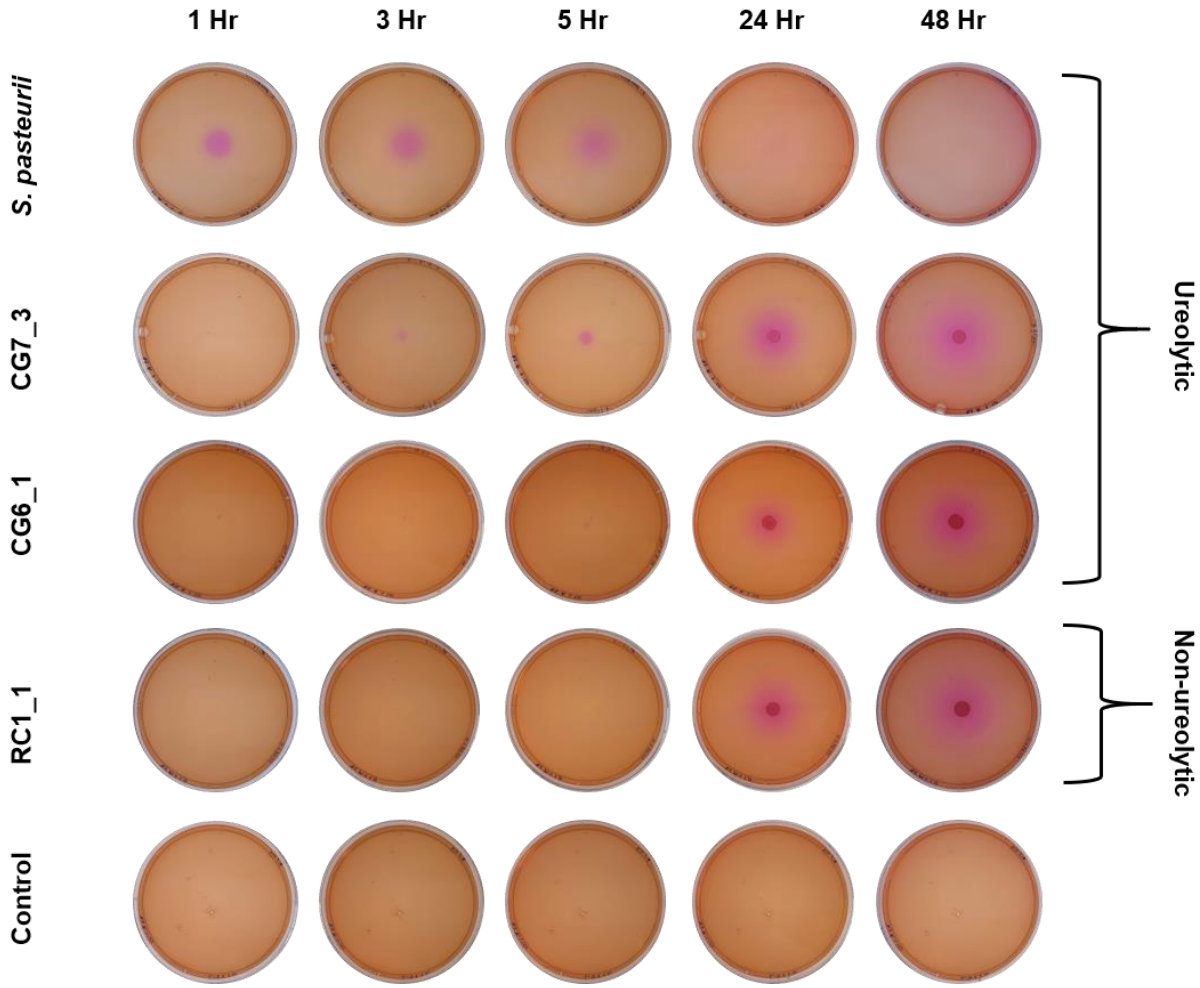

Figure S3. No pH changes are seen in ureolytic isolates when urea is excluded from the media. Nutrient agar plates supplemented with phenol red and calcium acetate were inoculated in the centre with suspensions of the same strains. Only local pH changes characteristic of normal metabolism are seen.

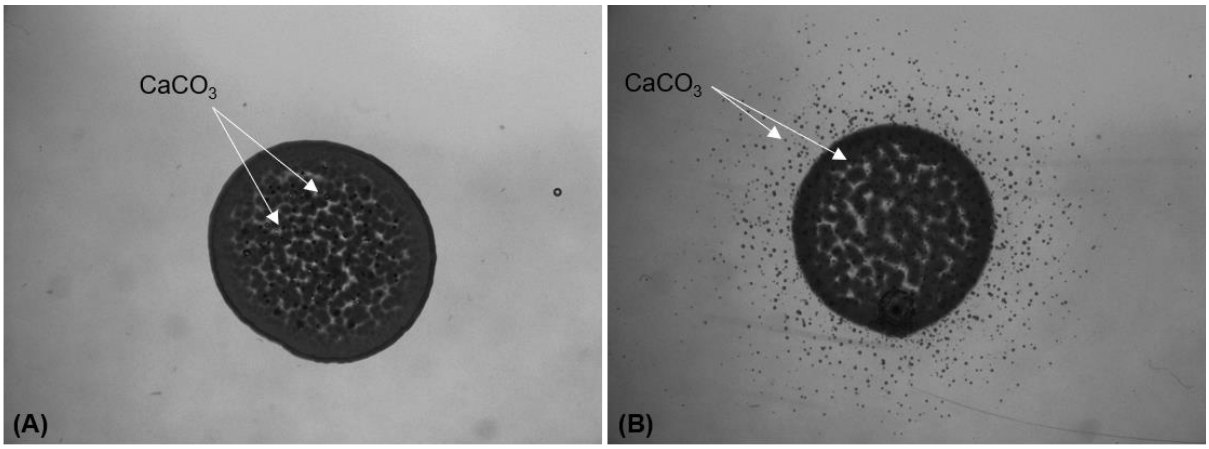

Figure S4. Comparison of crystal localisation in ureolytic strain CG7_3 without (A) and with (B) urea. Ureolytic bacteria precipitate crystals locally in the absence of urea, similar to what is seen in non-ureolytic strains. Arrows indicate $CaCO_3$ crystals.

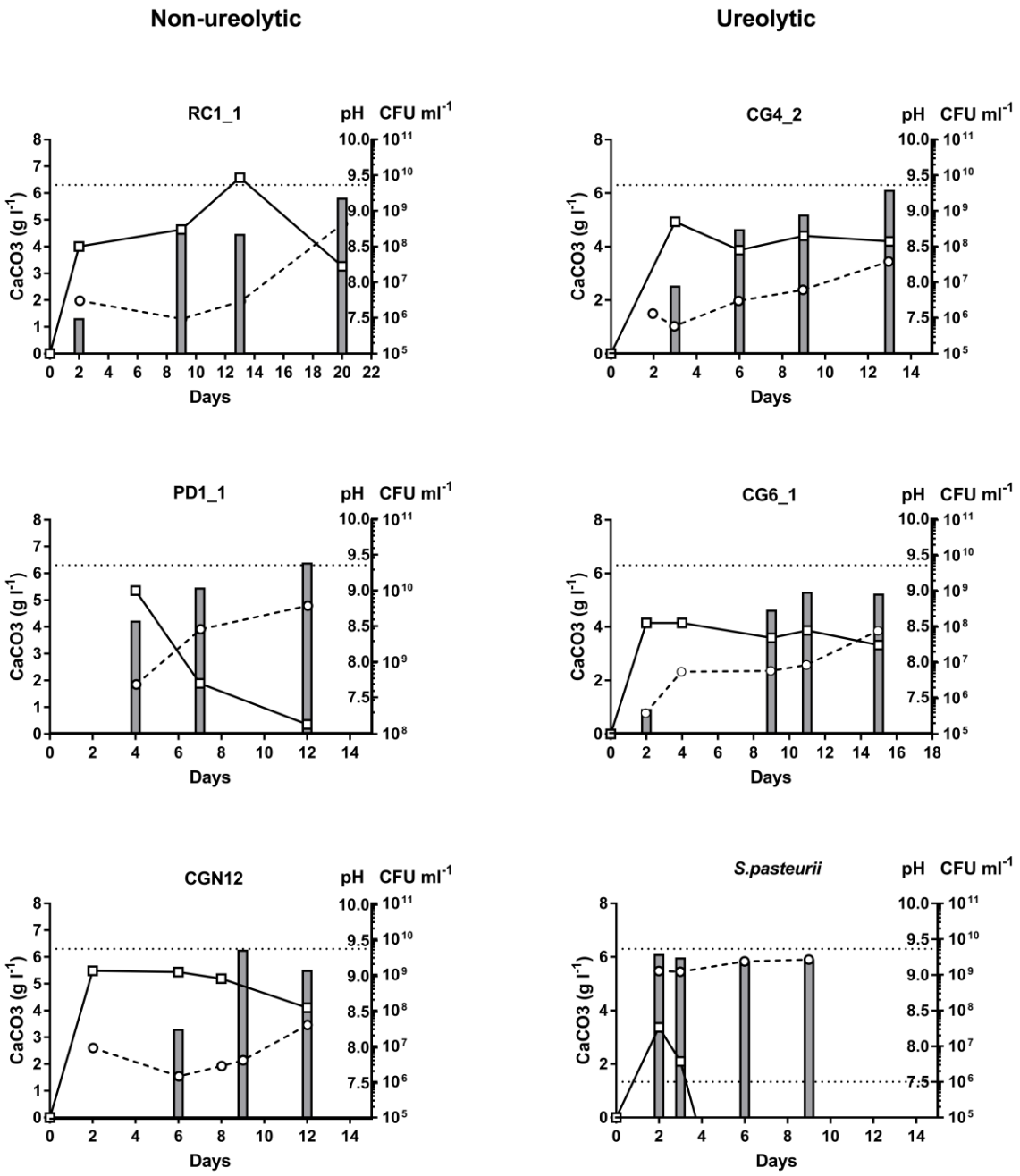

Figure S5. Calcite precipitation kinetics in ureolytic and non-ureolytic isolates. Isolates were grown in LB medium supplemented with urea (20 g l^{-1}) and CaAoc (10 g l^{-1}) and precipitation of insoluble calcium carbonate (bars, g l^{-1}), pH changes (circles) and changes in cell number (boxes, CFU ml^{-1}) were monitored over time (days).

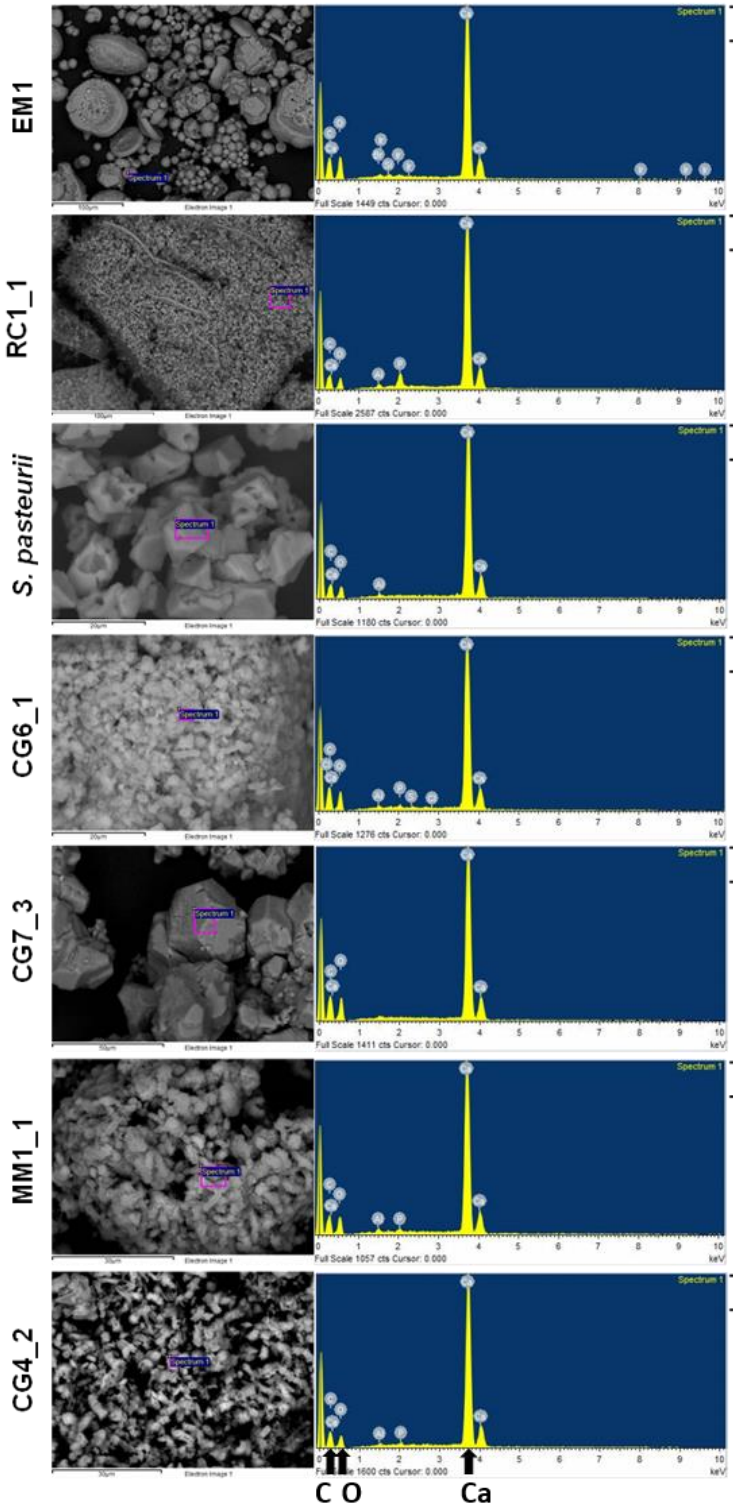

Element	Weight%	Atomic%
C	18.32	30.10
O	40.64	50.12
Ca	39.33	19.36
Totals	**98.29**	**99.58**

Element	Weight%	Atomic%
C	17.80	31.62
O	30.01	40.02
Ca	48.85	26.00
Totals	**96.66**	**97.64**

Element	Weight%	Atomic%
C	15.27	27.27
O	33.90	45.44
Ca	50.50	27.03
Totals	**99.67**	**99.74**

Element	Weight%	Atomic%
C	20.26	33.38
O	36.40	45.03
Ca	42.26	20.87
Totals	**98.92**	**99.28**

Element	Weight%	Atomic%
C	20.38	32.83
O	39.55	47.83
Ca	40.08	19.35
Totals	**100.00**	**100.00**

Element	Weight%	Atomic%
C	18.06	30.50
O	36.47	46.25
Ca	44.29	22.42
Totals	**98.82**	**99.17**

Element	Weight%	Atomic%
C	17.69	31.06
O	32.09	42.31
Ca	49.25	25.92
Totals	**99.03**	**99.29**

Figure S6. EDX analyses of precipitates produced by environmental bacteria. *Left,* the position on the precipitate where EDX was conducted (purple boxes). *Centre*, corresponding EDX spectra are shown, with the three peaks of main components labelled below. *Right,* elemental analysis indicating that the three main components (%) of the precipitate where carbon (C), oxygen (O), and calcium (Ca). Minor elements were excluded from the summary tables.

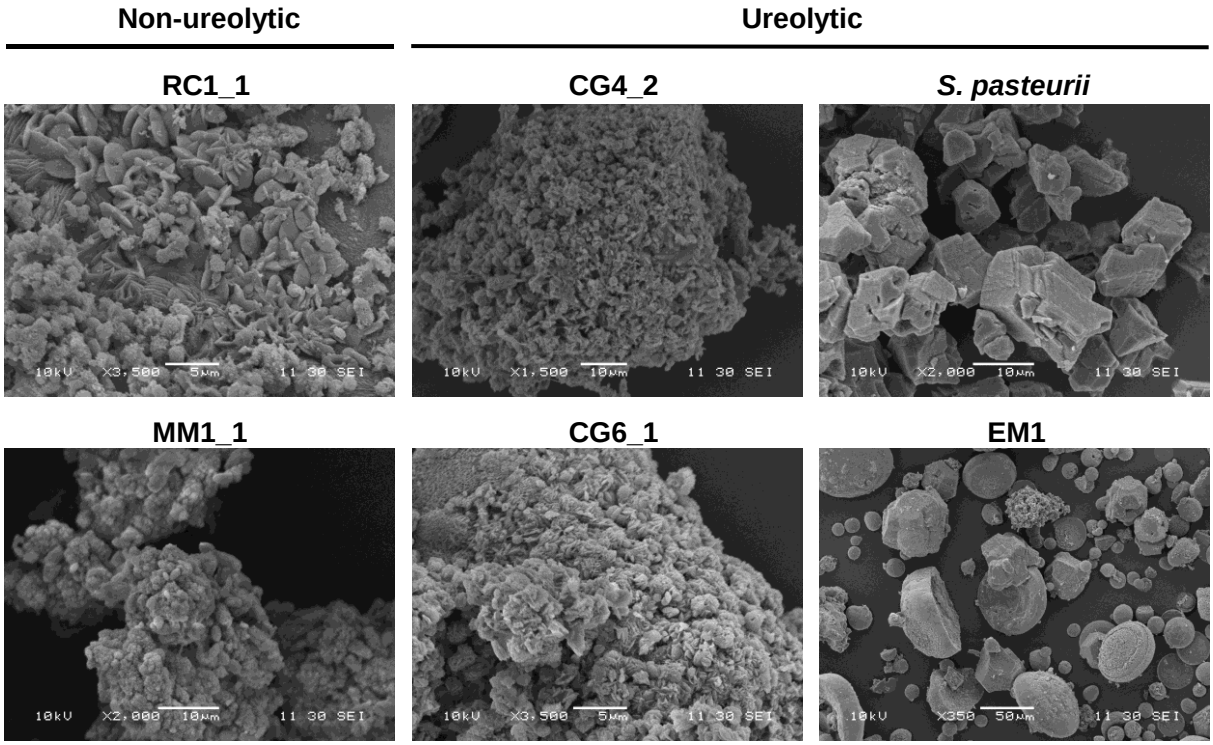

Figure S7. Crystal morphology in ureolytic and non-ureolytic isolates. Isolates were grown in LB medium supplemented with urea (20 g l^{-1}) and $Ca(OAc)_2$ (10 g l^{-1}) and electron micrographs of representative precipitates were taken between days 9-15. Strain names and their ureolytic potential are stated above.

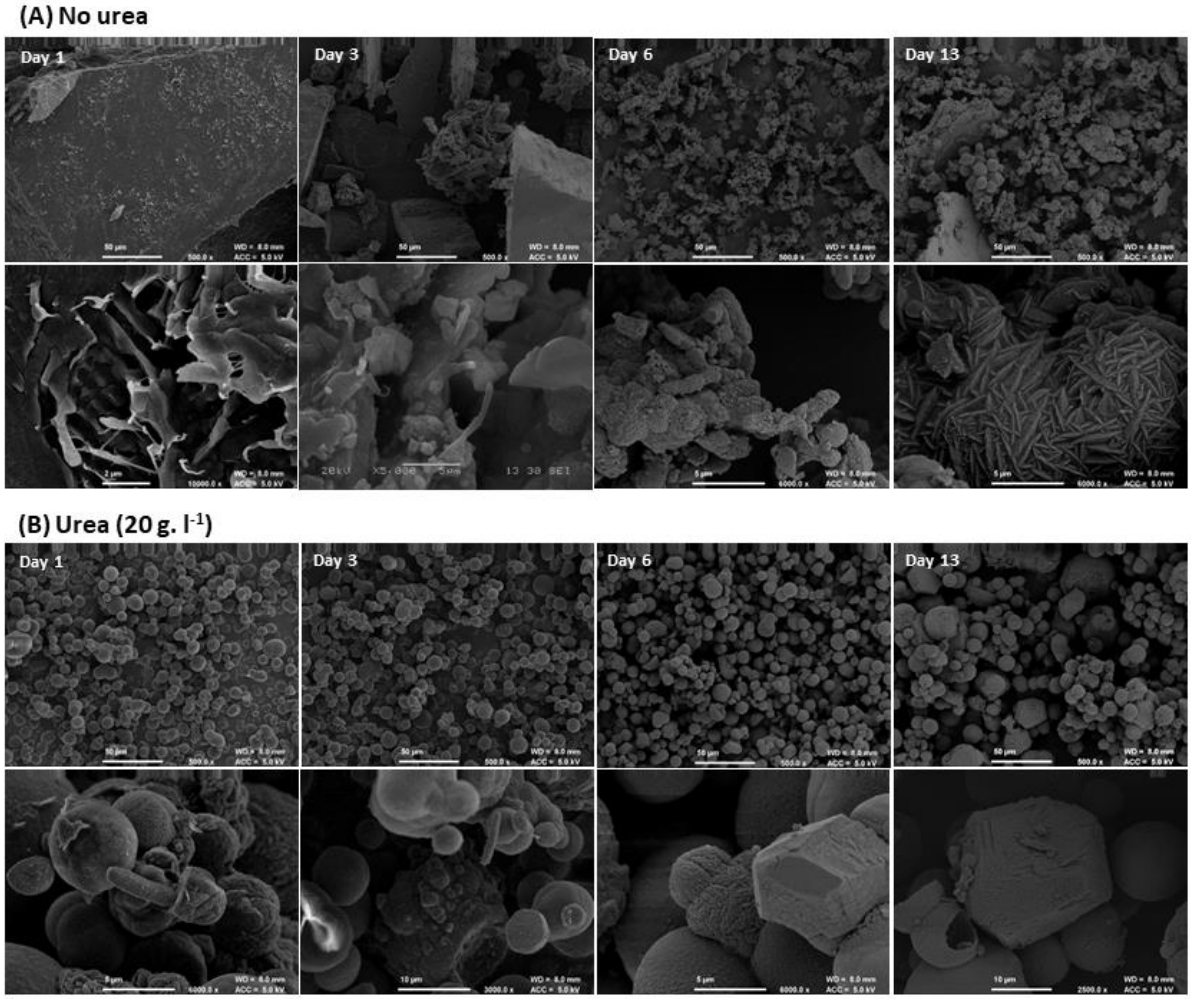

Figure S8. Comparison of crystal morphology in CG7_3 grown in the absence and presence of urea. The ureolytic strain CG7_3 was grown in LB medium supplemented with $Ca(OAc)_2$ (10 g l^{-1}) in the absence (A) and presence (B) of urea (20 g l^{-1}). Electron micrographs of precipitate were taken at days 1,3, 6 and 13. The top panel of each series represents a low magnification view, the bottom panel a high magnification close-up.

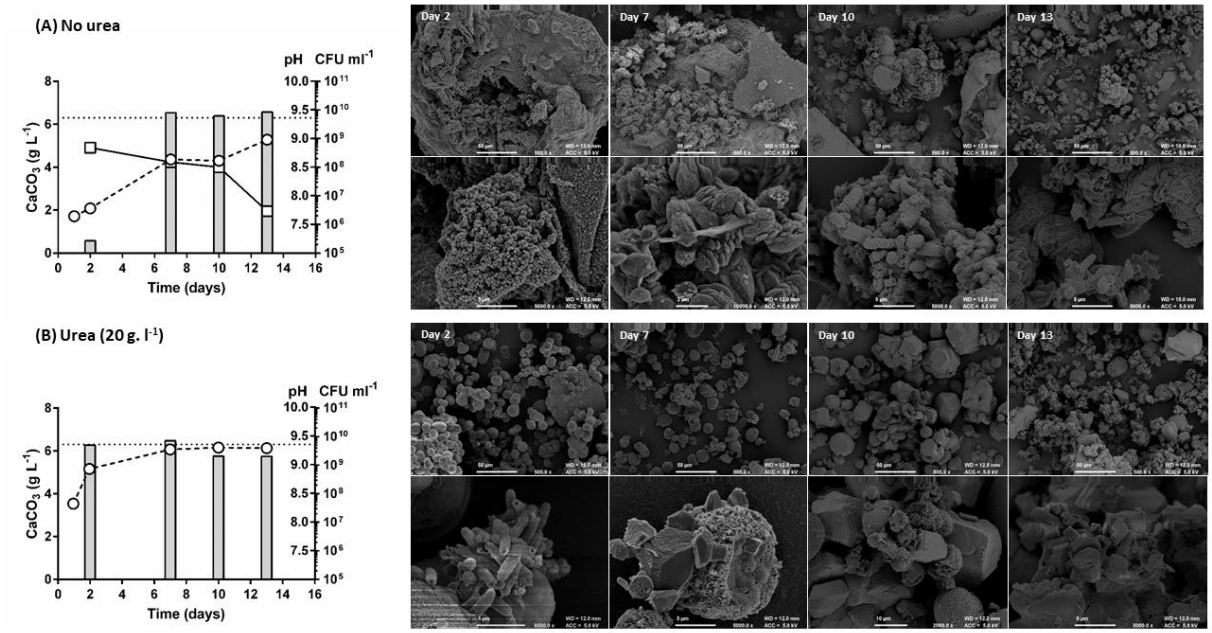

Figure S9. Comparison of ureolytic and non-ureolytic mechanisms of calcite precipitation in CG7_3. Ureolytic strain CG7_3 was grown in LB medium supplemented with $Ca(OAc)_2$ (10 g l^{-1}) in the absence (A) and presence (B) of urea (20 g l^{-1}). Precipitation of insoluble calcium carbonate (bars, g l^{-1}), pH changes (circles) and changes in cell number (boxes, CFU ml^{-1}) were monitored over time (days). *Right,* electron micrographs of representative precipitate taken at days 2, 7, 10 and 13.